Earth Evolution Sciences, Vol. 11, pp. 3-22, March, 1, 2017

Mineralogy of Gondwana Sequence in Barapukuria Formation, Bangladesh

Ismail Hossain[1,2,*], Toshiaki Tsunogae[2,3], Md. Sultan-Ul-Islam[1], Rita Rani Roy[1] and Shawon Talukder[4]

[1]*Department of Geology and Mining, University of Rajshahi, Rajshahi 6205, Bangladesh*
[2]*Graduate School of Life and Environmental Sciences (Earth Evolution Sciences), University of Tsukuba, Ibaraki 305-8572, Japan*
[3]*Department of Geology, University of Johannesburg, Auckland Park 2006, Johannesburg, South Africa*
[4]*Geological Survey of Bangladesh (GSB), Pioneer Road, Segunbagicha, Dhaka, Bangladesh*

** Corresponding author: Ismail Hossain*
E-mail address: ismail_gm@ru.ac.bd (I. Hossain)
Phone: +88-0721-750974, Mobile: +88 01741243440, Fax: +88-0721-750064

Abstract

The present research deals with mineralogy of Gondwana sequence from Barapukuria Formation, Bangladesh. Petrography, XRD, SEM and EPMA have been utilized to identify minerals with their mineralization processes, provenance, paleoclimate and post-depositional changes of rocks. Mineral assemblages indicate significant clay minerals of mixed-layered illite-smectite, kaolinite, chlorite, sericite, laumontite with quartz, opal-CT, feldspar, muscovite, pyrite and limonite. The overall clay mineral assemblages of the sequence reveal the sub-aerial mechanical and chemical weathering of the source rocks under sub-humid to humid climatic condition. Although kaolinite indicates consistent result, chlorite may be low grade metamorphic alternation mineral of existing ferromagnesium minerals, and opal-CT produced mainly volcanogenic origin rather than biogenic source. However, dominantly present illite-smectites, especially in lower portion of the thick coal seam signify their inherent were gradually converted volcanic materials to K-bentonites. The volcanic events (e.g., tuffaceos deposits) that yielded major illite-smectite deposits are linked with supereruptions, which affected the global climate. These types of genetic events of illite-smectites have also been reported worldwide. In the Tethyan region, the Cambrian-Ordovician orogenesis might have been actively contributed such type of materials during the assembly of Gondwana supercontinent. Signatures of volcanogenic materials (tuffite) have enormous value as stratigraphic marker horizons in this Indian subcontinent and very important stratigraphic markers. These finding is significant not only for their value in local and regional chronostratigraphic correlation but also for global geochronology, paleotectonic and paleoclimatic reconstructions.

Keywords: Illite-Smectite, Ordovician K-bentonites, Laumontite, Glass shard, Gondwana supercontinent.

Introduction

In Bangladesh, the Gondwana deposits are identified in the Kuchma, Jamalgonj, Barapukuria, Khalaspir, Singra, Phulbari, Dighipara and Burirdoba basin (Uddin and Islam, 1992; Islam, 1996; Hossain et al., 2002). In these basins, merely Barapukuria Gondwana sequence is the most prominent and well studied sedimentary deposits in Bangladesh. The Barapukuria is the first underground coal mine in Bangladesh, which first discovered by Geological survey of Bangladesh in 1985. Tectonically the Barapukuria basin is located in the Rangpur saddle/stable platform characterized by shallowest occurrence of the basement. Geographically the Barapukuria coal basin is located near the Barapukuria village under Parbatipur thana, Dinajpur district, Bangladesh and is bounded between latitude 25°31′28″ N and 25°34′40″ N and Longitude 88°56′36″ E and 88°59′02″ E (Fig. 1). Although several sedimentological and structural studies on the Gondwana sequence of the Barapukuria Formation are available (e.g., Islam et al., 1987; Wardell Armstrong Ltd, 1991; Islam et al., 1992; Uddin and Islam, 1992; Hossain, 1999; Hossain et al., 2000; Islam, 2001; Islam and Hossain, 2006; Farhaduzzaman et al., 2012), no systematic mineralogical study has so far been reported from the basin.

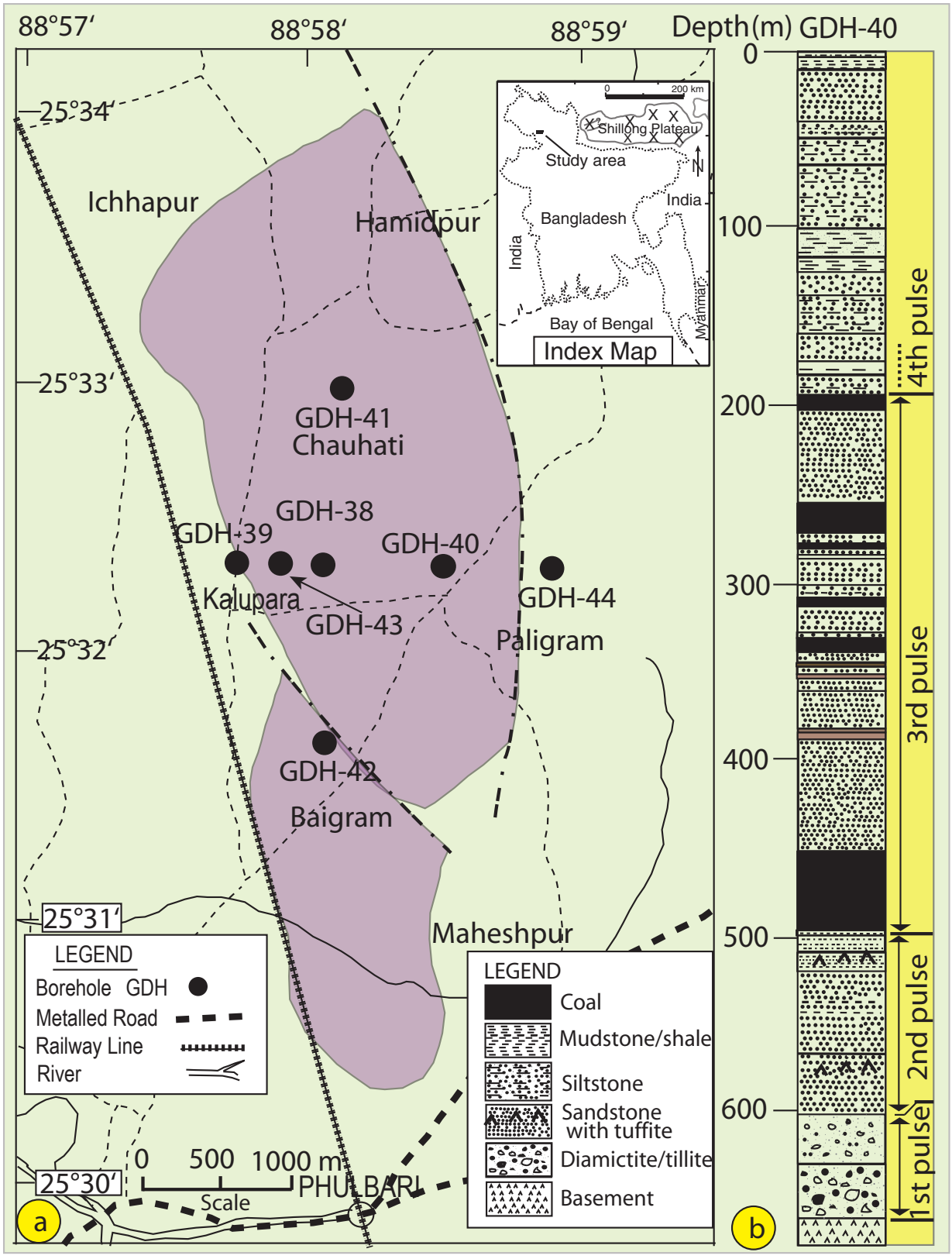

Fig. 1 (a) Location map of the study area showing Barapukuria basin area with boreholes position (slightly modified from Hossain, 1999), and (b) representative Litholog (GDH-40) showing lithological variation with multi-pulses sections.

X-ray Diffraction (XRD), Optical Petrography, Scanning Electron Microscopy (SEM) and Electron Microprobe Analyzer (EPMA) are applied for understanding mineralogical characteristics and to interpret the genesis of minerals of Gondwana deposits. The present study is aimed to identify the clay minerals and their mineralization with detrital minerals, and to interpret their genesis as well as tectonics and paleoenvironmental conditions of Gondwana deposits in the Barapukuria basin.

Geological setting

The shelf region of the Bengal Basin is an alluvial plain with slightly elevated terraces that slope towards south and south east. In this region, sedimentary rocks range in age presumably recorded from Permo-Carboniferous, through Jurassic and Cretaceous, to Tertiary and Quaternary which is overlaying the Paleoproterozoic (1.73 Ga) Basement rocks (Hossain et al., 2007). The overlying cover consists of successive units of the Permian Gondwana Formation, Pliocene Dupi Tila Formation, Pleistocene Barind Clay Formation and recent alluvium. The Gondwana Formation is concealed by the ubiquitous cover of about 100 to 200 m of Tertiary sediments (mainly Dupi Tila Formation). A large gap in sedimentary record is present in between Gondwana Group and Dupi Tila Formation, which are most probably happened due to the erosion or non-depositional phase exist during Triassic to Pliocene age (Islam, 1994, 2001). The sedimentary rocks of Gondwana sequence, Dupi Tila Formation, Barind Clay, and alluvium of the Early Permian, Pliocene, Pleistocene and Recent ages respectively are present on the Paleoproterozoic basement rocks. Tectonically the Barapukuria coal basin is located in the Rangpur saddle/stable platform. In the saddle area, Tertiary rocks overlie the Basement complex in most of the areas except in the basin areas like Barapukuria, Khalaspir, Burirdoba etc. basins, where in between Gondwana sequences are present. Sub-surface stratigraphic succession of Barapukuria basin with Rangpur saddle and adjoining area were summarized in the Table 1. The coal bearing Gondwana basins have been discovered in gravity lows/subsided basin areas in the Rangpur saddle and adjoining areas (Islam, 1994). The Barapukuria basin is a self-contained half-faulted graben controlled sedimentary basin, thought to be one of the subsided basins/grabens within the basement (Islam, 1992). It is believed that these grabens were formed as a result of post-Gondwana rifting in the Gondwana supercontinent (Khan and Chouhan, 1996). These types of basins are also identified in cratonic area of India and these basins are thought to be down-warped blocks of the platform in the basement complex. These types of basins are also reported from South Africa, Australia, Antarctica etc (Bakr et al., 1996).

The stratigraphic succession and structure of this basin has been established on the basis of borehole data and seismic survey (Bakr et. al., 1986; Islam et al., 1987; Wardell Armstrong Ltd, 1991; CMC, 1994). The Gondwana rocks of the basin form an asymmetric syncline

Table 1 Stratigraphic succession of the Barapukuria basin with surrounding Rangpur Saddle and adjoining areas of the Shelf zone, Bengal Basin (modified after Bakr et. al., 1996, Hossain, 1999; Islam, 2001, Hossain et al., 2007; CMC, 1994).

Age	Shelf (Bogra Slope) Group/Formation	Rangpur Saddle Group/Formation	Barapukuria Basin Group/Formation	Lithological description
Recent	Alluvium (78m)	Alluvium (53m)	Alluvium (2m)	Sand, silt and clay
Pleistocene	*Barind Clay (15m)	Barind Clay (15m)	Barind Clay (10m)	Yellow-brown sticky clay, sandy clay
Middle Pliocene to Late Miocene	Dupi Tila (270m)	Dupi Tila (171m)	Upper Dupi Tila (148m)	Mottled, sticky yellowish, brown clay with ferruginous nodules.
			Lower Dupi Tila (80m)	Dirty white clayey sand, sandy kaolinitic claystone, mudstone, white clay.
Early Miocene	Jamalganj (Surma Gr. undiff) (413m)	Surma Gr. undiff (?) (125m)		Fine to medium grained sandstone, sandy and silty shale, siltstone, shale.
Oligocene	Bogra (163m)			Siltstone, carbonaceous shale and fine grained sandstone.
Late Eocene	Kopili (43m)	Tura sandstone (?) (128m)		Sandstone, locally glauconitic and highly fossiliferous, shale with the calcareous bands.
Middle to late Eocene	Sylhet Limestone (197m)			Nummulitic limestone with sandstone interbeds.
Middle Eocene to Paleocene	Tura Sandstone (104m)			Gray and white sandstone with subordinate, greenish grey shale and coal.
Late Cretaceous	(Sibganj Fm) Trapwash (131m)			Coarse yellow brown sandstone, volcanic material, white clay.
Late Jurassic to Middle Cretaceous	Rajmahal Trap. (305m)			Amogdaloidal basalt, Serpentinized shale and agglomerate.
Permian (?)	Paharpur Formation (421m) Raniganj Group	Gondwana Group (475m)	Barapukuria Formation (457m) Gondwana Group	Feldspathic sandstone, carbonaceous and ferruginous sandstone, siltstone, shale/mudstone, Sandstone interbedded with 3~4 beds of tuffite, Diamictite/tillite/conglomerates and coal beds..
	Kuchma Formation (494m) Barakar Group			
Paleoproterozoic	Basement Complex	Basement Complex	Basement Complex	Diorite, quartz diorite, gneiss, schist, amphibolite.

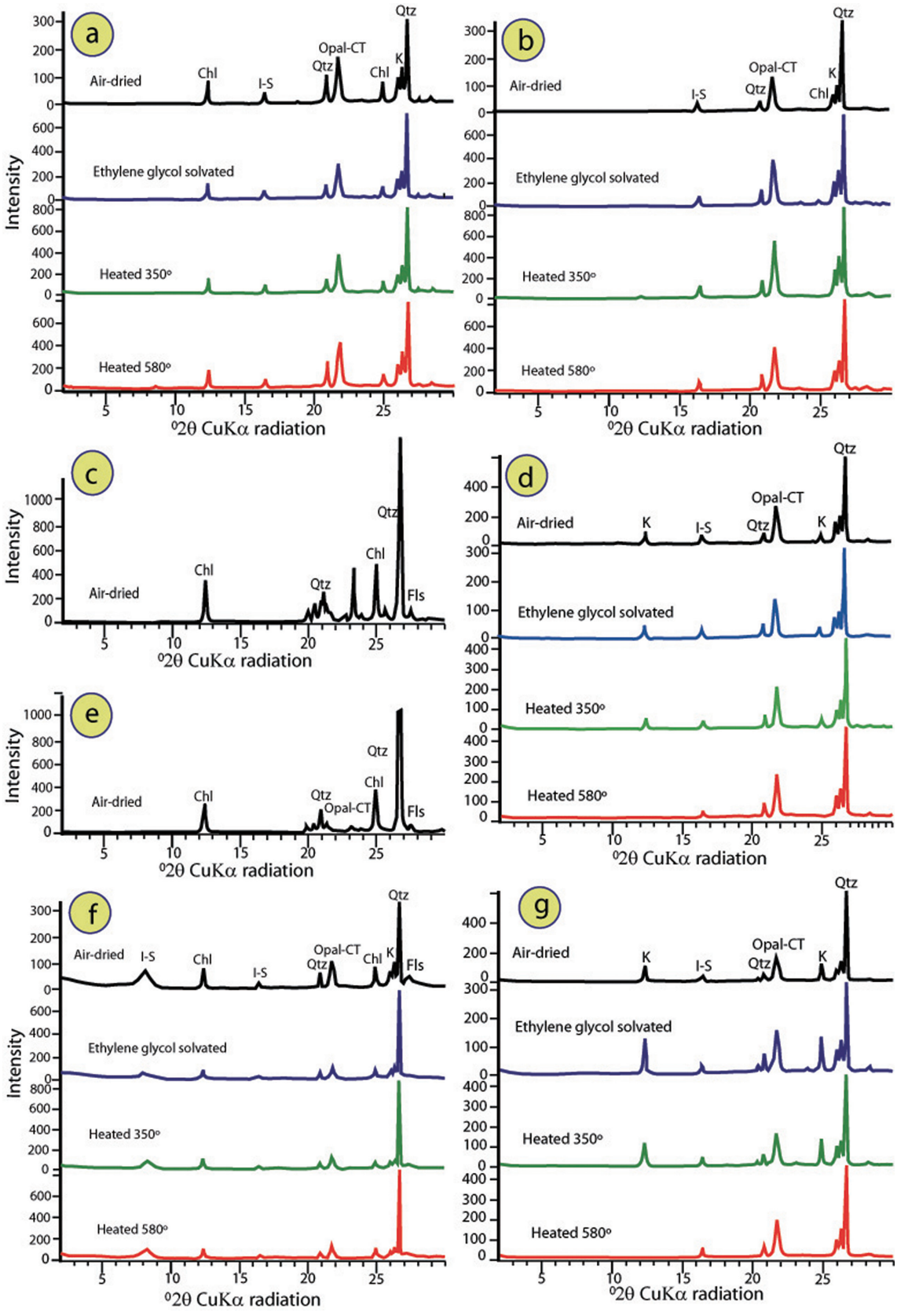

Fig. 2 XRD data showing peak intensity of Illite-Smectite (I-S), Chlorite (Chl), Kaolinite (K), Quartz (Qtz), Opal-CT and Feldspar (Fls) at depth 194 m in GDH-40 (a), 205 m in GDH-41 (b), 251 m (c), 317 m (d), 348 m (e), 474 m (f) and 487 m in GDH-40 (g).

along N-S direction having eastern boundary faults (CMC, 1994). The lowermost glacial and fluvio-glacial sediments are resting unconformable on the denuded basement complex. Above this diamictite/tillite, thick, predominantly continental arenaceous sediments with a number of coal seams are present.

Methods of study

About 1200 m cored Gondwana sequence from three boreholes (GDH-40, GDH-41 and GDH-43) are studied in detailed in order to prepare lithologs of studied boreholes on the basis of gross lithology, internal homogeneity of sedimentary texture and sedimentary structures. Some petrographic thin sections were prepared for petrographic study. Moreover, the following methods have also been applied for detailed study of the Permian Gondwana sequence:

X-ray Diffraction (XRD): Mineralogical analyses were carried out by XRD on powders of seven bulk sediments of Permian Gondwana rocks from boreholes GDH-40 and GDH-41 in the Barapukuria coal basin. Most of these sandstones and a mudstone samples were primarily broken and separated clay fractions by sieving method. Isolation of clay-sized fractions started with drying and gentle crushing of the mudstone, after which specimens were immersed in 3% H_2O_2 for at least 24 hrs to digest organic matter. We then added ~250 ml of Na-hexametaphosphate solution and inserted beakers into an ultrasonic bath for several minutes to promote desegregation and deflocculation. This step (and additional soaking) was repeated until visual inspection indicated complete desegregation. After transferring the suspended sediment to a 60-ml plastic bottle, each sample was re-suspended by vigorous shaking. The clay aggregates were saturated with ethylene glycol vapor for at least 24 hrs prior to XRD analysis, using a closed vapor chamber heated to 60°C in an oven. The analytical work was carried out for the identification of clay minerals using XRD technique at the laboratory of the Geological Survey of Bangladesh (GSB), Dhaka. It is noted that the smear method is acceptable mounting method for preferentially orienting clays (Gibbs, 1965). Most clay and associated minerals mounted in a preferential orientation can be identified by scanning from $2^0 2\theta$ to $30^0 2\theta$ (Cukα radiation). Generally, the preferentially oriented mount gives more sensitive data than do randomly oriented mounts. The clay samples in oriented mounts were run by a PHILIPS X-Pert PRO X-ray diffractometer with Ni filtered CuKα radiation using 40kV-40 mA. Samples were X-rayed using Ni-filter CuKα radiation with a scan range from 4^0 to 30^0 2θ, a step size of 0.2^0 and a dwell time of 1 second per step and were run under four separate conditions. The X-ray patterns were recorded in natural conditions (air-dried state), after ethylene glycol treatment, and after heating at 350^0C and 580°C for 1 hour.

Scanning Electron Microscopy (SEM): Morphological aspects of the clay particles were investigated on three samples using Scanning Electron Microscopy (SEM–HITACHI® S-3000 N) at the University of Tsukuba, Japan.

Electron Microprobe Analysis (EMPA): Chemical analyses of minerals in Gondwana sedimentary rocks were carried out by electron microprobe analyzer (JEOL JXA-8621) at the Chemical Analysis Division of the Research Facility Center for Science and Technology, the University of Tsukuba, Japan. The analyses were performed under conditions of 20 kV accelerating voltage and 10 nA sample current, and the data regressed using an oxide-ZAF correction program supplied by JEOL. The results of representative analysis of minerals are given in Tables 3, 4, 5, 6 and 7.

Results

General Petrography of Gondwana Group

The Gondwana Group of the studied boreholes encountered five lithostratigraphic units throughout the continuation from the base. These are diamictite/tillite, alteration of fine to medium-grained sandstone, gritstone, pebbly gritstone and dark gray siltstone, interbedded with 3~4 beds of tuffite, carbonaceous and ferruginous sandstones, thick coal seam VI and associated basal sequence, monotonous feldspathic sandstone, and pebbly/gritty sandstone, siltstone, mudstone with coal seam I-V (Hossain, 1999; CMC, 1994). The sandstones are mostly coarse to fine-grained and moderately to poorly sorted. On average the sandstones comprise of 42% quartz, 12.1% feldspar, 1.7% rock fragments, 14% organic matter, 5.3% matrix and 37.2% authigenic cements (Hossain et al., 2000). Sandstones shows different varieties based on the thickness of sediments. Generally lower portion of the coal seam VI displays sub-arkose with few sub-litharenite, whereas, those of the upper part are arkosic arenites or arkose and sub-arkose.

Optical microscopy of the sandstone samples of lower portion of the coal seam VI display mainly of quartz, K-feldspar and clay minerals with few accessory phases such as muscovite and limonite. Relict textures of precursor volcanic glass are only seldom preserved (Fig. 4h). Although clay minerals typically display flaky, columnar, pore-filling, elongate particles with irregular shapes, in situ and massive types, we assume that volcanic glass was the precursor for most of the clay minerals present in these sandstones/mudstones. In some cases, altera-

tion of muscovite or feldspar phenocrysts contributes to the clay mineral assemblage (Fig. 3b). A variation in the compositional components from bottom to top of the sequence was identified (Hossain, 1999). Quartz is irregularly variable in response to rock types throughout the sequence. Feldspar content gradually increases and matrix gradually decreases from base towards top of the Gondwana sequence. Other components comparatively

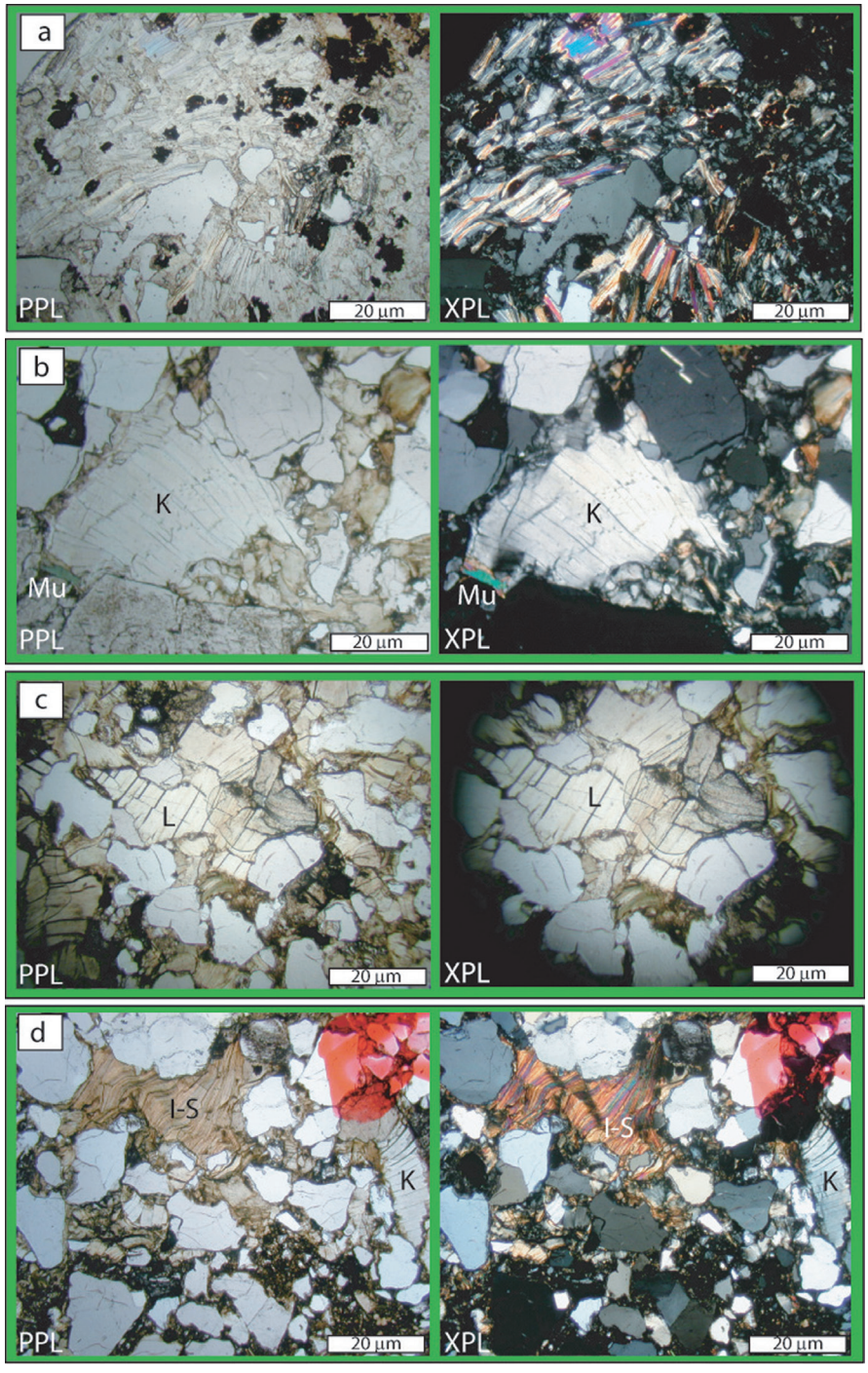

Fig. 3 Microphotographs showing (a) clay minerals indicate previous flow direction which might be volcanic ash flow, (b) Kaolinite (K) formed after deposition indicated by quartz grain which is surrounded by kaolinite and their cleavage not affected by quartz grain, and muscovite (Mu) changed to kaolinite, (c) laumontite (L) cement, and (d) Illite-smectite (I-S) and kaolinite formed in a single spot.

static or varies irregularly. XRD analysis of bulk samples indicates that the sandstones/claystone consists mainly of illite-smectite, kaolinite and chlorite clay minerals with lesser amounts of quartz, opal-CT and feldspar (Table 2).

Mineralogy

Clay minerals: Clay mineral abundance of the Gondwana sequence ranges from 3 to 19% of the rock volume in sandstone samples, averaging 9% of the rock volume (Hossain, 1999). Based on optical characteristics, the interpreted clay mineral assemblage is usually dominated by kaolinite, illite-smectite and rare chlorite, sericite. Authigenic clays make up a majority of the total clay within these sandstones. Authigenic clays occur as alteration products, rims around detrital grains, pore-linings (Fig. 3d) and pore-filling cement. Most clay minerals occur as scattered pore fillings. All over the sequence, considerable amount of clay cement and clay as alteration products are also present. In some cases, clay as alteration of feldspar (e.g., kaolinite) and rarely volcanic grains (e.g., glass shard) are also present. Generally clay minerals are a group of hydrous aluminosilicates with the majority having sheet silicate structures and consist of composite layers stocked along the c-axis. The composite layers are composed of sheets of cations (chiefly Al^{3+}, Fe^{3+}, Mg^{2+} and Fe^{2+}) in octahedral co-ordination with oxygen and hydroxyl anions, linked to sheets of Si^{4+} (with some substitution by Al^{3+} and to a lesser extent Fe^{3+} and Ti^{3+}) in tetrahedral co-ordination with oxygen and hydroxyl anions. There may be one of each layer type (1:1) two tetrahedral layers plus one central octahedral layer (2:1) or two 2:1 composite layer with an additional octahedral layer between them 2:1:1. XRD analysis of seven (7) samples has shown that illite-smectite, kaolinite, chlorite, quartz, opal-CT and feldspar are present in the most samples (Table 2).

Mixed-layered Illite-Smectite: Mixed-layered illite-smectite is reported first time from the Gondwana sedimentary rocks in Bangladesh. Mixed-layered clay minerals are those in which individual crystals are composed of unit cells or basic unit layers of two or more types. It is reasonably possible that the great majority of clay minerals are composed of interstratified layers of differing composition. Illite-Smectite is a regular mixed-layer type, which composed of alternating mica-like and smectite-like layers. SEM analyses revealed that illite-smectite morphologies are of very fine, irregular, curved flakes or mats of coalesced flakes (Figs. 3d and 4f). In general, flakes seem to be anhedral, but it was difficult to determine their exact texture because of particle coalescence. These clay mineral morphologies are typical for illite-smectite, which might be the minerals from bentonite (e.g., Keller et al., 1986). Throughout the

Table 2 XRD analyses of clay dominant lithology of different boreholes with their minerals.

Sample No.	Boreholes	Depth (m)	Lithological descriptions	List of minerals from XRD Analysis
S_4	GDH-40 (Fig. 2a)	193.55	Feldspathic, gritty and carbonaceous sandstone, carbonaceous shale/ claystone with clay	Chlorite, Illite-Smectite, Quartz, Opal-CT, Kaolinite
S_5	GDH-41 (Fig. 2b)	205.07	Dark grey to dull black carbonaceous fine-grained sandstone, composed of quartz, mica and dark minerals, medium hard with clay	Illite-Smectite, Quartz, Opal-CT, Kaolinite, Chlorite
S_3	GDH-40 (Fig. 2c)	251.46	Black colored silty clay	Chlorite, Quartz, Feldspar
S_2	GDH-40 (Fig. 2d)	317.30	Light greyish black to black, medium to fine-grained carbonaceous sandstone, compose of quartz with clay	kaolinite, Illite-Smectite, Quartz, Opal-CT
S_1	GDH-40 (Fig. 2e)	348.08	Medium to very coarse-grained, gritty sandstone, at places conglomeratic with clay	Chlorite, Quartz, Feldspar, Opal-CT
S_6	GDH-40 (Fig. 2f)	474.27	Greenish grey granules to pebble sized sandstone, composed of quartz and feldspar, partly decomposed, sandy matrix with clay	Chlorite, Illite-Smectite, Kaolinite, Quartz, Opal-CT, Feldspar
S_7	GDH-40 (Fig. 2g)	487.07	Dark, greenish grey fine-grained sandstone, composite of quartz, feldspar, mica with clay	Kaolinite, Illite-Smectite, Quartz, Opal-CT

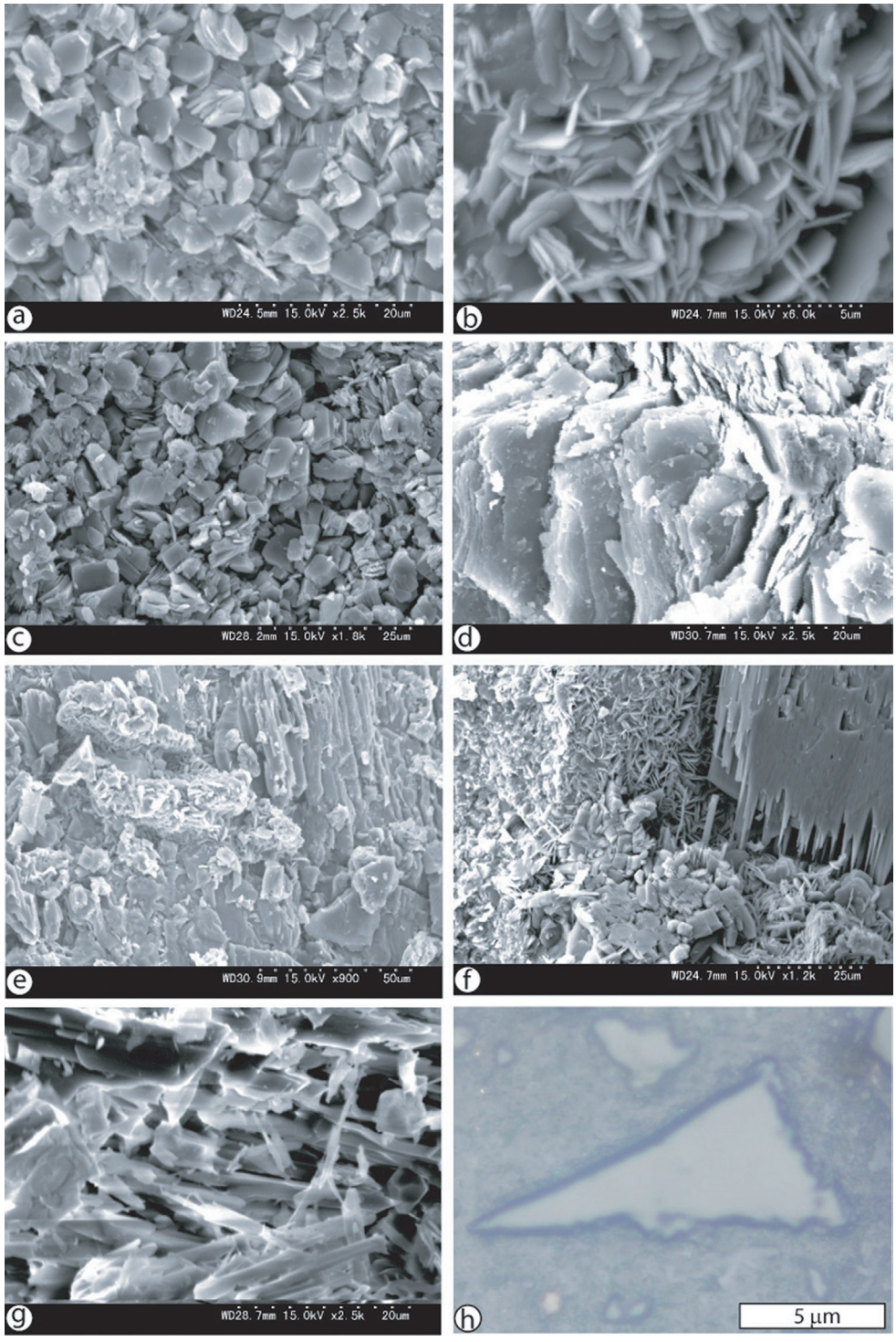

Fig. 4 SEM images show (a) initial and advanced stages of illitization of vermicular aggregates of kaolinites. Kaolinite exhibits typical booklet crystal morphology that is the result of precipitation as cement. Kaolinite cement reduces effective porosity and occludes intergranular pore spaces. The increased specific surface area of the kaolinite cement results in elevated irreducible water saturation. Sample depth = 605 m, (b) perfect Fe-Chlorite occurring as perpendicular rosettes of well-formed crystals on detrital grain surfaces, (c) commonly present Kaolinite + (Chlorite) at depth 576 m, (d) illite at depth 560 m, (e) feldspar and chlorite, (f) mixed-layer illite-smectite (left side), Fe-chlorite (center) and feldspar (upper right cornar) and kaolinite (lower middle) with mixed chlorite or illite-smectite. Precipitation of the clay mineral cement has resulted in the formation of microporosity (center). Pore-lining Fe-chlorite exhibits typical bladed rosette crystal morphology that is the result of precipitation as cement. Chlorite cement reduces effective intergranular porosity and occludes pore throats (sample depth = 576 m), (g) coal/organic matter, and (h) Microphotograph showing glass shard at depth 576 m.

Gondwana sequence, it is represented in XRD profiles by 002/003 labeled for ethylene glycol-solvated condition and shows reflection near 16.4°2θ (5.39Å) as the illite/EG-smectite, whereas in normal air dried condition display near 16.5°2θ (5.384Å) (Moore and Reynolds, 1989; Figs. 2a, 2b, 2d, 2f and 2g). Normally mixed-layered clay minerals have great difficulty to interpret their XRD patterns. In this case, heat treatments and solvation with water and ethylene glycol (EG) methods can be significance to identify mixed-layered species successfully.

Petrography and Chemistry of Mixed-layer Illite-Smectite: Petrographic and mineral chemical information provide significant amount of illite-smectite (Fig. 3d) in the studied rocks. Illite-smectite occurs as pore-linings and pore-filling cement. Occasionally it occurs as clay rims on detrital grains. It is also seen as the product of detrital grain alteration. Illite-smectite is present in minor amounts in most samples. Petrographic photographs rarely demarcate clear flow direction which might be the primary volcanic ash flow direction, that later transformed to illite-smectite. Indication of volcanic ash flow is only present at depth 560 m (Fig. 3a) in the borehole GDH-40. But these petrographic signatures very scatter and only present lower part of the thick coal seam. These volcanic materials are very much remarkable paleogeographic marker in this region. Petrographic and XRD data reveal the presence of highly abundance illite-rich I-S (>50% I) interstratified clay mineral in Gondwana rocks, which is the most conspicuous issue of its genesis and stability.

Chemical analyses (Table 3) show that the illite-smectites consist mainly of SiO_2, Al_2O_3, MgO, and FeO*, with lesser amounts of TiO_2, Na_2O, and CaO. The composition of the studied mixed-layered illite-smectite is listed in the Table 3. Major oxides are SiO_2 (avg. 43.10 wt.%) and Al_2O_3 (avg. 32.54 wt.%), whereas some FeO* (avg. 5.17 wt.%.), TiO_2 (avg. 0.32 wt.%), MgO (avg. 1.06 wt.%) and CaO (avg. 0.05 wt.%) present considerably. Illite-smectite mineral chemical data is very much supportive to estimate their formation temperature. In this case, Cathelineau (1988) proposed the formula T°C= -61.9229+321.9772 x Al^{IV}, where tetrahedral site Al is mainly change during the fluctuation of temperature of their formation. Application of the formula for the studied illite-smectite mineral chemical data, the estimated temperatures range from 175

Table 3 Mineral chemistry of illite-smectite

Spot No.	**I-S17**	**I-S28**	**I-S33**	**I-S34**	**I-S42**	**I-S43**	**I-S44**	**I-S45**	**I-S62**
SiO_2	41.549	39.978	44.193	45.418	42.714	43.043	43.356	43.828	43.858
Al_2O_3	30.980	30.965	35.060	34.847	32.415	30.786	33.078	33.102	31.660
TiO_2	0.356	0.203	0.086	0.096	0.309	0.932	0.352	0.423	0.134
Cr_2O_3	0.072	0.030	0.000	0.070	0.061	0.000	0.000	0.009	0.000
FeO	4.264	5.000	3.251	3.182	6.289	8.744	6.010	6.714	3.106
MnO	0.044	0.038	0.000	0.031	0.051	0.085	0.058	0.075	0.024
MgO	1.005	0.519	0.585	0.624	1.451	2.430	1.246	1.417	0.220
CaO	0.073	0.063	0.075	0.077	0.043	0.052	0.035	0.033	0.041
Na_2O	0.073	0.191	0.064	0.258	0.083	0.087	0.070	0.084	0.076
K_2O	1.613	0.903	0.491	0.605	1.512	2.027	1.104	1.201	0.604
ZnO	0.000	0.018	0.013	0.029	0.000	0.060	0.000	0.021	0.003
Total	**80.001**	**77.908**	**83.818**	**85.237**	**84.928**	**88.246**	**85.309**	**86.907**	**79.726**
Si	3.143	3.104	3.134	3.173	3.075	3.039	3.088	3.078	3.263
Al^{iv}	0.857	0.896	0.866	0.827	0.925	0.961	0.912	0.922	0.737
Sum T	**4.000**	**4.000**	**4.000**	**4.000**	**4.000**	**4.000**	**4.000**	**4.000**	**4.000**
Al^{vi}	1.906	1.938	2.065	2.042	1.825	1.600	1.864	1.819	2.039
Ti	0.020	0.012	0.005	0.005	0.017	0.049	0.019	0.022	0.007
Fe^{3+}	0.108	0.130	0.077	0.074	0.151	0.206	0.143	0.158	0.077
Fe^{2+}	0.162	0.195	0.116	0.112	0.227	0.310	0.215	0.237	0.116
Mn	0.003	0.002	0.000	0.002	0.003	0.005	0.003	0.004	0.002
Mg	0.000	0.000	0.000	0.000	0.000	0.000	0.000	0.000	0.000
Sum C	**2.199**	**2.277**	**2.263**	**2.235**	**2.223**	**2.171**	**2.244**	**2.240**	**2.241**
Ca (+Mg)	0.119	0.065	0.068	0.071	0.159	0.260	0.135	0.151	0.028
Na	0.011	0.029	0.009	0.035	0.012	0.012	0.010	0.011	0.011
K	0.156	0.089	0.044	0.054	0.139	0.183	0.100	0.108	0.057
Sum B	**0.286**	**0.184**	**0.121**	**0.160**	**0.309**	**0.454**	**0.245**	**0.270**	**0.096**

to 247°C. However, the plots of chemical variables of illite-smectite versus estimated temperature have been applied for recognizing their trends, some variables such as Fe, (Mg+Ca) and K are positively correlated with temperature, whilst it shows negative trend with Al^{VI}. So, it is remarkable that the most of the variables from the study area exhibits strong temperature dependence (Figure not shown).

Kaolinite: Kaolinite is very common clay mineral in the studied Gondwana sedimentary rocks. It occurs in two different modes, especially pore filling kaolinite that was directly precipitated within the individual pore space and in situ alteration of feldspar or muscovite that developed by alteration and replacement product of feldspars and/or muscovite (Fig. 3b). It is also commonly associated with feldspar dissolution. Kaolinite also occasionally occurs as booklets composed of stacked pseudohexagonal platelets (Fig. 4a and 4c). Some kaolinite cement precipitated before significant framework grain dissolution as suggested by kaolinite precipitation adjacent to secondary pore space, while kaolinite mostly replaces feldspar grains (Fig. 3d).

It is represented in XRD profiles by 001 and 002 basal reflections at about 12.39°2θ (7.10Å) and 24.87°9θ (3.56Å) (Moore and Reynolds, 1989; Figs: 2a, 2b, 2d, 2f and 2g). In general, kaolinite does not react with solvation since it does not have an expanding lattice and interlayer cation to solvate. Upon heating the mineral at 350°C, there is no change in the XRD pattern, though heating at 580°C may promote dehydroxylation ($2OH^- + Heat = O^{2-} + H_2O$). As the clay is completely dehydroxylate at 580°C, subsequently the structure of the mineral and its basal reflections are destroyed (Millot, 1970), which is a typical diagnostic treatment for kaolinite. Most of kaolinites in the studied samples are found poorly crystalline, which are reflected in the diffraction patterns by the broadening and weakening of the peaks and a tendency for adjacent reflections to fuse, most kaolinite have the 002 peak at 24.9°2θ and 12.5°2θ.

Kaolinite Chemistry: Kaolinite is a hydrous aluminium silicate of dioctahedral minerals containing minor amounts of other constituents. The composition of the studied kaolinites $Al_4(Si_4O_{10})(OH)_4$ is listed in the Table 4. Major oxides are SiO_2 (avg. 44.56 wt.%) and Al_2O_3 (avg. 35.08 wt.%), whereas some FeO* (avg. 2.09 wt.%.), TiO_2 (avg. 0.09 wt.%), MgO (avg. 0.42 wt.%) and CaO (avg. 0.07 wt.%) present considerably. Generally TiO_2 content is good indicator for the size of clay fraction. The values range from 0.013 to 0.135 wt.% TiO_2, which indicate more than 10 micron size of the clay fraction (Weaver and Pollard, 1975; Gribb and Banfield, 1997). The TiO_2 content of kaolinite is apparently dependant on the source mineral. When feldspar is the major source or the clay is of hydrothermal origin, the TiO_2 content of the kaolinite is low, when the source is biotite schist or biotite granite the TiO_2 content is relatively high. Occasionally the studied kaolinite contains considerable amount of FeO* rang-

Table 4 Mineral chemistry of kaolinite and sericite

Spot No.	K1	K2	K3	K4	K5	K8	K9	K10	K11	K40	K41	K46	K47	S56	S57
SiO_2	44.728	43.732	44.605	42.779	43.799	43.628	43.614	43.449	45.962	45.643	45.471	46.043	45.814	53.516	57.451
Al_2O_3	35.812	34.393	35.525	34.898	34.281	34.164	34.271	34.270	34.624	35.848	36.276	36.049	35.643	18.639	19.148
TiO_2	0.000	0.068	0.056	0.049	0.025	0.182	0.216	0.064	0.314	0.054	0.068	0.030	0.027	0.000	0.074
Cr_2O_3	0.036	0.059	0.023	0.000	0.028	0.004	0.022	0.000	0.000	0.035	0.000	0.009	0.009	0.004	0.000
FeO	1.387	1.835	1.390	1.391	1.105	2.813	3.629	2.507	2.788	2.218	2.206	1.772	2.093	7.238	1.834
MnO	0.000	0.000	0.000	0.000	0.025	0.021	0.021	0.000	0.041	0.034	0.027	0.007	0.000	0.000	0.000
MgO	0.295	0.307	0.462	0.400	0.345	0.394	0.456	0.522	0.268	0.869	0.641	0.263	0.224	0.288	0.065
CaO	0.090	0.054	0.111	0.082	0.065	0.090	0.087	0.064	0.135	0.016	0.013	0.018	0.027	0.016	0.02
Na_2O	0.039	0.045	0.077	0.055	0.046	0.055	0.036	0.054	0.130	0.139	0.104	0.078	0.181	1.208	0.982
K_2O	0.192	0.170	0.263	0.233	0.187	0.768	0.701	0.394	0.853	0.424	0.410	0.230	0.212	10.094	10.954
ZnO	0.021	0.000	0.019	0.000	0.044	0.040	0.034	0.000	0.000	0.000	0.065	0.021	0.031	0.021	0.016
Total	**82.600**	**80.663**	**82.530**	**79.887**	**79.949**	**82.159**	**83.088**	**81.325**	**85.116**	**85.280**	**85.281**	**84.520**	**84.261**	**91.024**	**90.544**
Si	4.044	4.058	4.041	4.003	4.085	4.018	3.989	4.022	4.082	4.026	4.010	4.073	4.073	3.790	3.981
Al^{IV}	0.000	0.000	0.000	0.000	0.000	0.000	0.000	0.000	0.000	0.000	0.000	0.000	0.000	0.210	0.019
Sum T	**4.044**	**4.058**	**4.041**	**4.003**	**4.085**	**4.018**	**3.989**	**4.022**	**4.082**	**4.026**	**4.010**	**4.073**	**4.073**	**4.000**	**4.000**
Al^{VI}	3.816	3.761	3.793	3.849	3.768	3.709	3.695	3.739	3.624	3.727	3.771	3.758	3.735	1.346	1.545
Ti	0.000	0.005	0.004	0.003	0.002	0.013	0.015	0.004	0.021	0.004	0.005	0.002	0.002	0.000	0.004
Fe^{3+}	0.042	0.057	0.042	0.044	0.034	0.087	0.111	0.078	0.083	0.066	0.065	0.053	0.062	0.171	0.043
Fe^{2+}	0.063	0.085	0.063	0.065	0.051	0.130	0.167	0.116	0.124	0.098	0.097	0.078	0.094	0.257	0.064
Mn	0.000	0.000	0.000	0.000	0.002	0.002	0.002	0.000	0.003	0.003	0.002	0.001	0.000	0.000	0.000
Mg	0.040	0.042	0.062	0.056	0.048	0.054	0.062	0.072	0.035	0.114	0.084	0.035	0.030	0.030	0.007
Sum C	**3.960**	**3.951**	**3.964**	**4.017**	**3.906**	**3.994**	**4.051**	**4.009**	**3.890**	**4.011**	**4.024**	**3.926**	**3.922**	**1.806**	**1.662**
Ca	0.009	0.005	0.011	0.008	0.006	0.009	0.009	0.006	0.013	0.002	0.001	0.002	0.003	0.001	0.001
Na	0.007	0.008	0.014	0.010	0.008	0.010	0.006	0.010	0.022	0.024	0.018	0.013	0.031	0.166	0.128
K	0.022	0.020	0.030	0.028	0.022	0.090	0.082	0.047	0.097	0.048	0.046	0.026	0.024	0.912	0.968
Sum B	**0.038**	**0.034**	**0.055**	**0.046**	**0.037**	**0.109**	**0.097**	**0.063**	**0.132**	**0.073**	**0.065**	**0.041**	**0.058**	**1.079**	**1.098**
OH	8.087	8.116	8.082	8.006	8.170	8.037	7.979	8.044	8.163	8.052	8.021	8.145	8.147	1.806	1.662

ing from 1.105 to 3.629 wt.%. Stoichiometrical value of Fe_2O_3 (0.49 to 1.61 wt.%.) suggest both residual and sedimentary kaolinites present in the Gondwana sequence. Although it has not been established that any of the iron is in the kaolinite structure, the clays always have some iron suggesting that little amount is probably present in the structure. The ratio of SiO_2/Al_2O_3 (avg. 1.27) is as low as theoretical value of 200:100. The analysis of the kaolinites also gives A1/Si ratios significantly <1 (0.89 and 0.96) and lower interlayer occupancy (0.034 and 0.132). The compositional data do not correspond to ideal kaolinite, and the presence of interlayer cations indicates the occurrence of a mixture of kaolinite.

Chlorite: Optical petrographic results of the studied Gondwana rocks show very rare chlorite, especially lower portion of the thick coal seam. In the depth of 560, 576 and 605 m at GDH-40, there is no chlorite grains detected for a reliable chemical analysis. In general, it is difficult to obtain sedimentary chlorites of sufficient purity for reliable chemical analyses. However, reasonably accurate estimates of chlorite from XRD analyses are available. In the present study, chlorite found most of the samples at the upper portion of thick coal seam. This clay mineral is identified mainly by the peaks at about 12.38°2θ (7.14Å) and 24.89°2θ (3.27Å) (Moore and Reynolds, 1989; Figs. 2a, 2b, 2c, 2e and 2f). The diffractograph of air dried samples are not affected on glycolation and heat treatment up to 550°C for chlorite but those peaks are affected often weak and may not be detectable if the Cl concentration is low or if its Fe contain is high. Chlorite has a basal series of diffraction peaks based on a first order reflection of 12.2Å. The chlorite 004 is indicated for the peak at 25° 2θ. In SEM studies, the delicate nature of the chlorites have been exposed, under which those are seen to consist of small irregular hexagonal platelets, platy or cluster of bladed in pore fills, which display spectacular form of rosette (Fig. 4b). Generally Fe-chlorite shows most cases rosette nature, which is very common in the studied rocks.

Sericite: The term sericite is used to indicate highly birefringent, fine-grained dioctahedral micas that are viewed under the optical microscope. It is identified at depth 560 m in GDH-40. It is very unfortunate that we can not obtain any sericite data from XRD and SEM photographs. Sericite shows almost similar chemical composition as muscovite but generally have more SiO_2, MgO, H_2O and K_2O (Table 4). As the SiO_2 content increases, sericite approaches compositions similar to the illites and is referred to as a phengite or an alurgite (Weaver and Pollard, 1975). The chemistry of a single grain sericite from Barapukuria Gondwana sedimentary rocks show that it contains a higher content of K_2O (10.524 wt.%) and comparatively low MgO (0.177 wt.%). The structural formula of the sericite is $(K_{0.940}, Na_{0.147}, Ca_{0.001})$ $(^{VI}Al_{1.446}, Fe^{3+}_{0.107}, Fe^{2+}_{0.161}, Mg_{0.019})$ $(Si_{3.886}, ^{IV}Al_{0.114}, Ti_{0.002})$ O_{10} $(OH)_{1.734}$.

Laumontite: Laumontite, a zeolite group mineral, present locally in the sequence of the rock volume at depth 576 m in GDH-40. Generally the occurrences of laumontite as an intergranular cement or replaces grains (Fig. 3c), and fills fractures. Laumontite cements typically occur as optically clear, large poikilotopic patches, with well-developed cleavage and undulatory extinction. The cement is sometimes optically continuous, where laumontite cement is extensive, it occludes all visible porosity (Fig. 3c). Laumontite cement also fills intragranular pore spaces and fills through-going fractures to form veins. In some cases veins contain only laumontite whereas in other cases the veins contain scattered inclusions of detrital grains in addition to the laumontite. Laumontite cementation present in open fractures in the studied Gondwana rock and filling fractures within detrital grains. Laumontite cement occasionally occluded in authigenic silicate overgrowths line pore spaces.

Non-Clay Minerals

Quartz: Quartz is the most abundant minerals in the whole sequence of the studied Gondwana rocks. It constitutes about 10 to 75% of the total rock components, as detrital grains combining both monocrystalline and polycrystalline types. Quartz is also the most abundant mineral, which occurs as clay size particles in all the XRD analyzed samples and in consistently present throughout the studied depth range. This mineral is identified by the basal reflection at about 20.86°2θ (4.26Å) and 26.65°2θ (3.34Å) (Moore and Reynolds, 1989; Figs. 2a, 2b, 2c, 2d, 2e, 2f and 2g). In 26.65°2θ (3.34Å) reflection, the peak occasionally coincides with those of illite (3.4Å). The peaks have the strongest intensities; they do not alter on glycolation and heating.

Feldspar: Feldspar constitutes about 1 to 27% of the total rock components in the studied Gondwana sequence. Although feldspars are both potassium feldspar and plagioclase, lower part of the thick coal seam is very rare in species of plagioclase. Potassium feldspars range from 1 to 14% of the rock volume, averaging 6.2%. Orthoclase is the dominant variety, but microcline is also present in most samples. Many of these grains have been fractured or broken into smaller fragments due to compaction. Some grains have been partially dissolved to form secondary porosity while others have been altered to clay. The non-clay mineral feldspar is identified by the basal reflection at about 27.55°2θ (3.24Å) (Figs. 2c, 2e and 2f).

The peaks of the potassium feldspars are intense enough to show when feldspar is present in small amounts, while those are not found in the plagioclase series and that occur in the 2θ range normally used by clay mineralogist are the one at 27.45°2θ; two smaller ones at 21.10 and 25.65°2θ of microcline, and 21.05 and 25.75°2θ for orthoclase. The most intense line of orthoclase is at 26.75°2θ, which is often not usable as it is interfered with by the strongest quartz line at 26.65°2θ. Petrographic data show that the plagioclase ranges of trace to 2% in the rock volume and are almost absent in the depths from 560 to 605 m in GDH-40. Only potassium feldspar of these depth ranges were analyzed mineral chemistry (Table 5). In a few samples show pore spaces or grains replaced by calcite. Table 5 provides representative microprobe analyses of potassium feldspars of the studied Gondwana rocks. Analyzed potassium feldspar provides almost uniform orthoclase-rich composition in all samples (Or_{91-98} Ab_{2-9}).

Opal-CT: Opal-CT is interpreted as disordered microcrystallites of α-cristobalite in a matrix of amorphous silica (Guthrie et al., 1995). These crystallites exhibit varying degrees of stacking order, which may lead to the appearance of X-ray maxima that coincide with those of α-tridymite. Opal-CT has an XRD pattern characterized by two broad reflections in the 4.05 to 4.10Å and 2.50Å regions and a single small reflection at 4.25 to 4.35Å. The most intense Opal-CT reflection may occur anywhere from 4.07 to 4.10Å with peak widths ranging from 0.506Å to 0.883Å (Elzea et al., 1994). The breath and position of this peak are a consequence of the combination of two unresolved peaks, the α-cristobalite and α-tridymite like layers (Elzea and Rice, 1996). In some cases, a secondary peak with a position closes to the (404) α-tridymite line is observed on the high angle side of the main opal-CT reflection. Opal-CT is present in all samples of the study. It is identified by broad reflection at 21.95°2θ of corresponding d-spacing value 4.10Å (Figs. 2a, 2b, 2d, 2e, 2f and 2g).

Muscovite: Optically very common muscovite is colorless or pale shade, gray or slightly brown laminar masses or flakes at depths 560, 576 and 605 m in the studied Gondwana rocks. Results of the mineral chemistry of muscovite from EMPA data suggest their variable chemical composition (Table 6). SEM photographs show partly decomposed muscovite forming clay minerals. It is very remarkable that there is no muscovite peak from XRD data throughout the sequence. The chemical compositions of the four muscovites, obtained from EMPA analyses are compared in Table 7. The representative structural formulae for B6-7, B23-25, and B30-32 are almost identical in their Al contents. The number of ^{IV}A1 is 1.56-1.88 pfu and the number of ^{VI}A1 is 3.21-3.72 pfu. But B38-39 shows almost reverse result, e.g., ^{IV}A1 is 2.09-2.22 pfu and ^{VI}A1 is 0.63-0.67 pfu. Besides, the number of interlayer cations (K^+, Na^+ and Ca^+) is about 2 in only B30-32 with B6-7, B38-39 are near identical, but B23-25 is very poor (0.63-0.77). Such compositional ambiguities indicate not all muscovite end-member composition. In the case of first three grains some Fe was localized on the M site and thus (Al+Fe) = 4 pfu, leading to a sum of M-site cations greater than 2 (Table 6). In the case of a grain (B23, B24, B25 positions) interlayer site at 0.633, 0.634, and 0.773 was found probably indicating either the presence of a very

Table 5 Mineral chemistry of feldspar

Spot No.	F12	F13	F14	F15	F18	F19	F21	F22	F29	F35	F36	F37	F48	F49	F51	F52	F53	F59	F60	F61	F63	F64	F66	F67	F68
SiO^2	62.89	62.16	62.76	61.85	64.39	58.59	64.70	58.64	59.15	65.62	64.93	64.83	64.79	64.89	64.23	64.84	64.24	63.36	65.40	65.51	62.43	64.05	65.49	64.83	65.33
Al_2O_3	17.01	17.56	17.37	17.57	17.84	17.45	17.15	18.31	17.36	18.22	18.25	18.59	18.15	18.53	18.56	18.55	18.04	18.33	18.32	18.40	18.01	18.32	18.59	18.56	18.42
TiO_2	0.02	0.00	0.00	0.00	0.00	0.00	0.01	0.02	0.00	0.00	0.03	0.00	0.00	0.03	0.00	0.00	0.00	0.00	0.01	0.00	0.00	0.01	0.00	0.00	0.00
Cr_2O_3	0.00	0.01	0.03	0.04	0.00	0.00	0.01	0.00	0.00	0.00	0.00	0.00	0.00	0.00	0.02	0.01	0.03	0.01	0.00	0.00	0.00	0.02	0.00	0.00	0.05
FeO	1.12	0.03	0.04	0.05	0.04	0.05	0.00	0.06	0.01	0.01	0.00	0.02	0.05	0.03	0.00	0.05	0.05	0.04	0.04	0.04	0.04	0.06	0.09	0.05	0.07
MnO	0.00	0.00	0.00	0.02	0.00	0.00	0.00	0.00	0.02	0.00	0.02	0.00	0.00	0.00	0.03	0.00	0.00	0.05	0.00	0.00	0.04	0.05	0.01	0.00	0.00
CaO	0.01	0.00	0.01	0.00	0.00	0.01	0.00	0.00	0.01	0.00	0.00	0.00	0.00	0.00	0.00	0.00	0.00	0.00	0.01	0.00	0.00	0.00	0.00	0.01	0.00
Na_2O	0.70	0.63	0.66	0.63	0.80	0.78	0.94	0.68	0.75	0.96	0.68	0.83	0.23	0.72	0.93	0.92	0.88	0.64	0.53	0.63	0.85	0.65	0.58	0.71	0.72
K_2O	13.93	14.10	14.35	13.85	13.45	14.00	14.84	16.31	14.11	15.54	15.92	15.44	16.38	15.76	15.00	15.38	15.51	16.28	16.23	16.04	14.25	15.89	16.39	15.96	16.53
ZnO	0.02	0.00	0.06	0.04	0.03	0.01	0.09	0.00	0.00	0.07	0.00	0.04	0.02	0.00	0.00	0.03	0.01	0.01	0.01	0.00	0.00	0.00	0.03	0.00	0.03
Total	95.69	94.50	95.28	94.05	96.63	90.88	97.73	94.02	91.40	100.42	99.83	99.75	99.62	99.96	98.77	99.79	98.75	98.72	100.54	100.62	95.61	99.04	101.18	100.11	101.15
Si	3.02	3.01	3.02	3.01	3.04	2.97	3.04	2.92	2.98	3.01	3.00	2.99	3.01	2.99	2.99	2.99	3.00	2.98	3.01	3.00	3.00	2.99	2.99	2.99	2.99
Al	0.96	1.00	0.99	1.01	0.99	1.04	0.95	1.07	1.03	0.99	0.99	1.01	0.99	1.01	1.02	1.01	0.99	1.01	0.99	0.99	1.02	1.01	1.00	1.01	0.99
Ti	0.00	0.00	0.00	0.00	0.00	0.00	0.00	0.00	0.00	0.00	0.00	0.00	0.00	0.00	0.00	0.00	0.00	0.00	0.00	0.00	0.00	0.00	0.00	0.00	0.00
Cr	0.00	0.00	0.00	0.00	0.00	0.00	0.00	0.00	0.00	0.00	0.00	0.00	0.00	0.00	0.00	0.00	0.00	0.00	0.00	0.00	0.00	0.00	0.00	0.00	0.00
Fe^{3+}	0.00	0.00	0.00	0.00	0.00	0.00	0.00	0.00	0.00	0.00	0.00	0.00	0.00	0.00	0.00	0.00	0.00	0.00	0.00	0.00	0.00	0.00	0.00	0.00	0.00
Fe^{2+}	0.04	0.00	0.00	0.00	0.00	0.00	0.00	0.00	0.00	0.00	0.00	0.00	0.00	0.00	0.00	0.00	0.00	0.00	0.00	0.00	0.00	0.00	0.00	0.00	0.00
Mn	0.00	0.00	0.00	0.00	0.00	0.00	0.00	0.00	0.00	0.00	0.00	0.00	0.00	0.00	0.00	0.00	0.00	0.00	0.00	0.00	0.00	0.00	0.00	0.00	0.00
Ca	0.00	0.00	0.00	0.00	0.00	0.00	0.00	0.00	0.00	0.00	0.00	0.00	0.00	0.00	0.00	0.00	0.00	0.00	0.00	0.00	0.00	0.00	0.00	0.00	0.00
Na	0.06	0.06	0.06	0.06	0.07	0.08	0.09	0.07	0.07	0.09	0.06	0.07	0.02	0.06	0.08	0.08	0.08	0.06	0.05	0.06	0.08	0.06	0.05	0.06	0.06
K	0.85	0.87	0.88	0.86	0.81	0.91	0.89	1.03	0.91	0.91	0.94	0.91	0.97	0.93	0.89	0.91	0.92	0.98	0.95	0.94	0.87	0.95	0.96	0.94	0.97
Total	4.95	4.95	4.96	4.94	4.91	5.00	4.97	5.10	4.99	4.99	5.00	4.99	4.99	5.00	4.99	4.99	5.00	5.03	5.00	5.00	4.97	5.01	5.01	5.01	5.02
An	0.06	0.00	0.06	0.00	0.02	0.05	0.00	0.00	0.03	0.00	0.00	0.00	0.00	0.00	0.00	0.00	0.00	0.00	0.04	0.00	0.00	0.00	0.00	0.05	0.00
Ab	7.06	6.37	6.53	6.43	8.25	7.79	8.81	5.98	7.44	8.61	6.09	7.51	2.09	6.45	8.59	8.32	7.90	5.65	4.71	5.62	8.27	5.83	5.08	6.33	6.18
Or	92.88	93.63	93.41	93.57	91.73	92.16	91.19	94.02	92.54	91.39	93.91	92.49	97.91	93.55	91.41	91.68	92.10	94.35	95.25	94.38	91.73	94.17	94.92	93.62	93.82
	Or	Or	Mr	Mr	Mr	Mr	Or	Or	Or	Or	Or	Or	Or	Or	Or	Or	Or	Mr	Mr	Mr	Mr	Mr	Or	Or	Or

minor additional polytype or substantial stacking faults. All crystals investigated show a significantly less paragonitic component, except B31 and B32 data, which show Na concentrations about 0.11pfu.

The Fe contents show inconsistency of each grains but they display well correlated negative trend (R=-0.73) with Si, also tend to be somewhat higher in the Fe-rich fraction, probably owing to minor biotite contamination. The variation diagrams of Si with respect to A1, Fe, and Mg as analyzed by microprobe (Figure not shown) show remarkable differences between the chemical compositions of the four muscovite types. B31-33 muscovite has relatively low Mg contents and high Na, Al and Fe/(Fe+Mg) contents, whereas, the Ti content of all muscovite types is extremely low, except B38-39 and points toward post-magmatic origin (Speer, 1984), which is in agreement with our textural observations on the thin sections. The

Table 6 Mineral chemistry of muscovite

Spot No.	B6	B7	B23	B24	B25	B30	B31	B32	B38	B39
SiO_2	44.120	43.361	41.768	41.796	42.395	45.067	44.906	45.569	39.085	37.267
TiO_2	0.161	0.318	0.478	0.396	0.437	0.083	0.168	0.056	1.416	1.289
Al_2O_3	28.887	28.050	27.581	29.919	27.756	34.311	33.696	34.443	15.414	15.552
FeO	4.938	5.217	9.631	9.746	10.702	3.543	2.453	2.149	15.308	17.956
MnO	0.045	0.069	0.044	0.024	0.030	0.052	0.056	0.021	0.221	0.234
MgO	0.857	0.873	1.643	1.867	2.911	0.168	0.151	0.167	12.594	11.721
CaO	0.035	0.042	0.091	0.051	0.088	0.056	0.000	0.000	0.014	0.024
Na_2O	0.098	0.195	0.091	0.111	0.073	0.394	0.322	0.414	0.172	0.049
K_2O	8.784	8.743	3.070	3.183	3.960	10.628	10.821	11.252	9.096	7.800
Cr_2O_3	0.004	0.022	0.021	0.000	0.021	0.000	0.036	0.023	0.000	0.038
H_2O*	4.109	4.044	3.973	4.095	4.104	4.399	4.340	4.410	3.962	3.865
Subtotal	92.038	90.934	88.450	91.209	92.505	98.704	96.952	98.504	97.365	95.870
O=F,Cl	0.000	0.000	0.000	0.000	0.000	0.000	0.000	0.000	0.000	0.000
Total	92.038	90.934	88.450	91.209	92.505	98.704	96.952	98.504	97.365	95.870
Si	6.439	6.430	6.304	6.120	6.194	6.143	6.205	6.197	5.915	5.782
^{IV}Al	1.561	1.570	1.696	1.880	1.806	1.857	1.795	1.803	2.085	2.218
^{VI}Al	3.408	3.333	3.210	3.284	2.974	3.655	3.692	3.717	0.665	0.626
Ti	0.018	0.035	0.054	0.044	0.048	0.009	0.017	0.006	0.161	0.150
Cr	0.000	0.003	0.003	0.000	0.002	0.000	0.004	0.002	0.000	0.005
Fe	0.603	0.647	1.216	1.193	1.308	0.404	0.283	0.244	1.938	2.330
Mn	0.006	0.009	0.006	0.003	0.004	0.006	0.007	0.002	0.028	0.031
Mg	0.186	0.193	0.370	0.408	0.634	0.034	0.031	0.034	2.841	2.711
Zn	0.000	0.000	0.007	0.002	0.003	0.000	0.000	0.000	0.009	0.009
Ca	0.005	0.007	0.015	0.008	0.014	0.008	0.000	0.000	0.002	0.004
Na	0.028	0.056	0.027	0.032	0.021	0.104	0.086	0.109	0.050	0.015
K	1.635	1.654	0.591	0.594	0.738	1.848	1.907	1.952	1.756	1.544
	1.668	1.717	0.632	0.634	0.772	1.960	1.993	2.061	1.809	1.562
OH*	4.000	4.000	4.000	4.000	4.000	4.000	4.000	4.000	4.000	4.000
Total	17.890	17.936	17.497	17.568	17.746	18.068	18.029	18.067	19.452	19.423
Y total	4.221	4.220	4.864	4.934	4.973	4.108	4.035	4.006	5.643	5.861
X total	1.668	1.717	0.632	0.634	0.772	1.960	1.993	2.061	1.809	1.562
Al total	4.969	4.903	4.906	5.164	4.780	5.513	5.488	5.521	2.750	2.844
Fe/Fe+Mg	0.764	0.770	0.767	0.745	0.673	0.922	0.901	0.878	0.405	0.462
K+Na+2*Ca	1.674	1.723	0.647	0.642	0.786	1.968	1.993	2.061	1.811	1.566

Table 7 Chemical formulae of muscovites in Gondwana sedimentary rocks, Bangladesh.

No.	I	M	T
B6	$K_{1.635}Na_{0.028}Ca_{0.005}$	$Al_{3.408}Fe_{0.603}Mg_{0.186}Mn_{0.006}Ti_{0.018}$	$Si_{6.439}Al_{1.561}O_{20}(OH)_4$
B7	$K_{1.654}Na_{0.056}Ca_{0.007}$	$Al_{3.333}Fe_{0.647}Mg_{0.193}Mn_{0.009}Ti_{0.035}Cr_{0.003}$	$Si_{6.430}Al_{1.570}O_{20}(OH)_4$
B23	$K_{0.591}Na_{0.027}Ca_{0.015}$	$Al_{3.210}Fe_{1.216}Mg_{0.370}Mn_{0.006}Ti_{0.054}Cr_{0.003}Zn_{0.007}$	$Si_{6.304}Al_{1.696}O_{20}(OH)_4$
B24	$K_{0.594}Na_{0.032}Ca_{0.008}$	$Al_{3.284}Fe_{1.193}Mg_{0.408}Mn_{0.003}Ti_{0.044}Zn_{0.002}$	$Si_{6.120}Al_{1.880}O_{20}(OH)_4$
B25	$K_{0.738}Na_{0.021}Ca_{0.014}$	$Al_{2.974}Fe_{1.308}Mg_{0.634}Mn_{0.004}Ti_{0.048}Cr_{0.002}Zn_{0.002}$	$Si_{6.194}Al_{1.806}O_{20}(OH)_4$
B30	$K_{1.848}Na_{0.104}Ca_{0.008}$	$Al_{3.655}Fe_{0.404}Mg_{0.034}Mn_{0.006}Ti_{0.009}$	$Si_{6.143}Al_{1.857}O_{20}(OH)_4$
B31	$K_{1.907}Na_{0.086}$	$Al_{3.692}Fe_{0.283}Mg_{0.031}Mn_{0.007}Ti_{0.017}Cr_{0.004}$	$Si_{6.205}Al_{1.795}O_{20}(OH)_4$
B32	$K_{1.952}Na_{0.109}$	$Al_{3.717}Fe_{0.244}Mg_{0.034}Mn_{0.002}Ti_{0.006}Cr_{0.002}$	$Si_{6.197}Al_{1.803}O_{20}(OH)_4$
B38	$K_{1.756}Na_{0.050}Ca_{0.002}$	$Al_{0.665}Fe_{1.938}Mg_{2.841}Mn_{0.028}Ti_{0.161}Zn_{0.009}$	$Si_{5.915}Al_{2.085}O_{20}(OH)_4$
B39	$K_{1.544}Na_{0.015}Ca_{0.004}$	$Al_{0.626}Fe_{2.330}Mg_{2.711}Mn_{0.031}Ti_{0.150}Cr_{0.005}Zn_{0.009}$	$Si_{5.782}Al_{2.218}O_{20}(OH)_4$

variation of the Na content of the muscovites is attributed to solid solution between the end members muscovite and paragonite. Modern studies by Chatterjee and Froese (1975) and Eugster et al. (1972) have provided useful information about the phase relations and their temperature dependence in this system. It is concluded that the decreasing Na contents of muscovites must suggest a decrease of formation temperature. The variations of Fe, Mg, and Al with Si can be related to solid solution between the end members of muscovite and celadonite (Figure not shown). Si contents indicate higher crystallization temperature with low pressure conditions (Powell et al., 1983). Diagrams (Figure not shown) show a discontinuity in the relationships of Al and Fe with Si for eight Si-rich muscovites.

Mineralization

Clay minerals are good indicator of paleoclimates, mode of weathering, provenance, environment of deposition and post depositional changes experienced by the sediments (Zuther et al., 2000). It is noted that three principal processes involve for genesis of clay minerals, namely detrital inheritance, transformation and deposition. Weaver (1958) argued that the detrital origin of clay minerals is mainly reflecting the character of the source rock, although they are liable to be altered during the process of transportation and deposition. From XRD, Optical Petrography, SEM and EPMA studies have been carried out to understand composition and genesis of clay minerals with detritus. Overall results exhibit dominant mixed-layered illite-smectite, kaolinite, chlorite, sericite, laumontite with quartz, opal-CT, feldspar, muscovite, pyrite and limonite. Dominantly present mixed-layered illite-smectite clay minerals typically formed by illitization of smectite during burial diagenesis or hydrothermal alteration at elevated temperatures, especially illite-rich clay minerals (e.g., Środoń and Eberl, 1984; Velde, 1995). XRD data display illite-rich (at least ~55% of illite) mixed-layered illite-smectite in the studied rocks. It is also very common that kaolinite usually illitized completely (e.g., Środoń, 1979). McDowell and Elders (1980) stated that detrital muscovite alters to sericite (illite or I-S). In general, the reaction sequence with increasing temperature is: detrital muscovite → sericite (I-S or illite) → phengite→muscovite. These data suggest that I-S and/or illite have a stability field with respect to muscovite. Normally illitization reaction becomes detectable only at temperatures significantly higher than surface temperatures (Środoń, 1999; Perry and Hower, 1970). The studied illite-smectites show higher temperatures range from 175° to 247°C. The Gulf Coast sediments (Hower et al., 1976) provide the evidence of the reaction for illitization; smectite + K-feldspar (+ mica?) → I-S + chlorite + quartz. On the other hand, the occurrences of glassy materials in the studied Gondwana rocks also suggest that illite-smectite might also be formed during weathering of silicic glass at depth 560 m in GDH-40 (e.g., Gilg et al., 2003).

The occurrence of kaolinite in the studied Gondwana rocks suggests normal alteration of feldspar during diagenesis, though under some conditions it may be altered into illite or muscovite. The presence of authigenic kaolinites in the studied Gondwana rocks signifies the passage of acidic waters at some stage in the diagenetic condition of the rocks. However, the question of whether this water is produced by mudrock diagenesis at depth or in surface derived has been addressed by many workers merely on the basis of rather ambiguous circumstantial evidence (Baker and Golding, 1992). The stability of the kaolin-group minerals under weathering, hydrothermal and diagenetic conditions has been investigated extensively in recent years. The most commonly observed transformation of kaolinite under intensive weathering conditions is to hydrated alumina (gibbsite) and soluble silica (Velde, 1995). During burial of sedimentary rocks,

kaolinite is transformed into illite, chlorite, mixed-layer minerals and pyrophyllite (e.g. Velde, 1995; Frey, 1987; Ehrenberg and Nadeau, 1989). Some of the mineralogical transformations observed in natural systems, such as the kaolinite-to-illite transformation, can today be interpreted on the basis of experimental studies. Accordingly, the kaolinite to K-mica transformation was observed in laboratory experiments, reacting kaolinite with alkaline solutions (e.g. Huang, 1993; Bauer et al., 1998; Bentabol et al., 2003) or through the formation of serpentine-like phases, which reacted with KCl to form dioctahedral mica (Frank-Kamenetskii et al., 1990).

SEM and XRD data indicate mostly Fe-chlorite present in the studied Gondwana rocks, such type of Fe-chlorite is very common in sandstones owing to the presence of pore-lining/pore-filling Fe-chlorite, even in high depth/high temperature regimes in many basins of different ages. It is very remarkable that many high iron chlorites associated with sedimentary iron formations apparently have formed by direct precipitation (Weaver and Pollard, 1975). Where mixing between Fe-rich fresh waters and marine waters occur in transitional environments, the chlorite-bearing rocks are deposited. Moreover, post-depositional chlorite is a common component in marine sandstone, where it commonly forms from the alteration of volcanic materials or montmorillonite. These types of deposits are available in the Ordovician K-bentonite beds of the eastern United States (Weaver, 1989). As in many cases the burial and thermal histories seem to affect the chlorite distribution and thickness. Normally Fe-chlorite forms in deep burial (>80°C) condition. Sericite in the studied Gondwana rocks shows almost similar chemical composition as muscovite (Table 4). As the SiO2 content increases, sericite approaches compositions similar to the illites and is referred to as a phengite or an alurgite (Weaver and Pollard, 1975). Sericite is usually hydrothermal origin. Laumontite is generally cementation in open fractures in the studied Gondwana rock and filling fractures within detrital grains, which suggests laumontite precipitation, is a late-stage diagenetic event. Laumontite cement occasionally occluded in authigenic silicate overgrowths line pore spaces, also suggesting its later genesis. Generally it is formed in large amount in some tuffaceous sediments as an alteration product of glass and plagioclase, occasionally forming extensive beds of impure laumontite-rich rock. It is very clear that formation of the studied laumontite resembles hydrothermal processes in areas of intense volcanism with a typical sedimentary process (e.g., Koporulin, 2013). The origin of Opal-CT, the most prominent non-clay minerals in the studied XRD analysis, has been attributed to either biogenic or volcanogenic processes. Biogenic process involves deposition of silica rich test of organic matter with diagenetic alteration of Opal-A to Opal-CT (Murata and Larson, 1975; Hein et al., 1978). The alternation of volcanic glass to smectite appears to coincide with the transformation of biogenic Opal-A to Opal-CT (Compton, 1991). The initial silica rich solution and the pH within or outside the partially decomposed volcanic roots initiated the change from precipitation of Opal-CT to clinoptilite (Senkayi et al., 1987). Clay rich siliceous rocks transform to Opal-CT at greater burial depths (higher temperatures) and transform to quartz earlier (lower temperatures) than clay-poor siliceous rocks (Compton, 1991). Volcanogenic processes create Opal-CT during alternation of volcanic ash (Aftabuzzaman et al., 2013) and deposited at low temperature condition (Reynolds, 1970). Most probably illite-smectite clays formed by alteration of volcanic ash, presence of primary and secondary fluid inclusions in quartz grains and adjoining mixed-layered illite-smectite clay minerals and the preservation of primary melt inclusion (Fig. 5), testify to the occurrence of significant hydrothermal alteration (Gilg et al., 1999) of Barapukuria Formation. XRD data are also identified non-clay feldspar, indicating their detrital mode from igneous origin. Orthoclase is ordinarily more resistant than plagioclase when hydrothermal alteration is subjected to the rock. Muscovite chemistry display inconsistency of Fe in each grains but they display well correlated negative trend with Si, probably owing to minor biotite contamination but they have remarkable differences their chemical compositions of most muscovite types. The Ti content of most muscovite types is extremely low, and points toward postmagmatic origin (Speer, 1984). The variation of the Na content of the muscovites is attributed to solid solution between the end members muscovite and paragonite. Chatterjee and Froese (1975) and Eugster et al. (1972) have provided useful information about the phase relations and their temperature dependence in this system. It is concluded that the decreasing Na contents of muscovites must suggest a decrease of formation temperature.

Discussions and conclusions

Within the sequence, characterization of clay minerals with adjacent detrital minerals and understanding their genesis are very complex tasks in paleoenvironmental conditions of Barapukuria Formation, Bangladesh. For obtaining such messages, XRD, Optical Petrography, SEM and EPMA studies on clay minerals and detritus have been carried out. Petrographically clay minerals with dominant quartz, feldspar, rock fragments, mica, organic matter, matrix and some secondary minerals are common

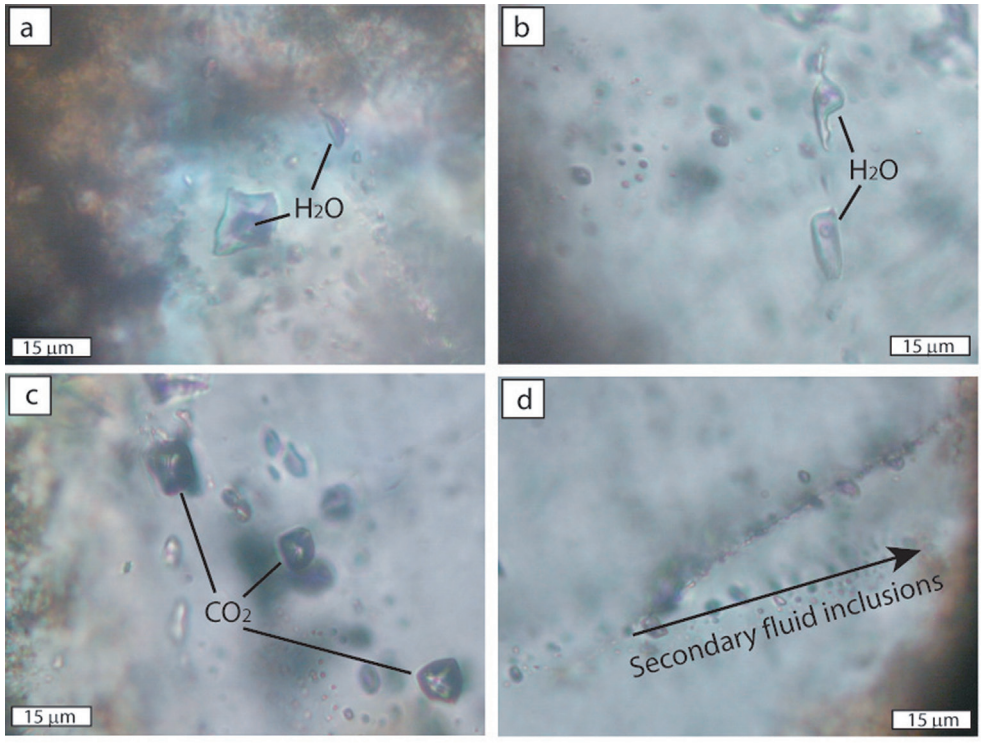

Fig. 5 Photomicrographs of representative fluid inclusions in this study: (a) fresh aqueous fluid inclusions in quartz, (b) glassy two-phase silicate melts inclusion of negative crystal shape in quartz, (c) carbonic fluid inclusions in quartz, and (d) secondary fluid inclusions also present in quartz grains.

in the studied sequence. Generally lower portion of the coal seam VI displays sub-arkose with few sub-litharenite, whereas, those of the upper part are arkosic arenites or arkose and sub-arkose. The XRD, SEM, Optical Petrography and EPMA analyses of the Gondwana rocks of the Barapukuria Formation provides clay mineral assemblages including significant mixed-layered illite-smectite, which elucidate modes of clay mineralization and their interrelationship along with their provenance, paleoclimate, paleoenvironments of deposition, mode of weathering and post-depositional changes. In the studied sequence has dominant clay minerals of mixed-layered illite-smectite (at least ~55% illite) with chlorite and kaolinite, whereas, quartz, opal-CT and feldspar are non-clay fractions. Mixed-layered illite-smectite, chlorite, opal-CT and quartz are commonly present throughout the sequence. Visual estimates of mineral content from the XRD patterns imply that the abundance of chlorite has not been significantly affected by the disappearance of kaolinite, nor the K-feldspar was completely lost. The clay content does not vary significantly with depth.

Dominantly present mixed-layered illite-smectite generally forms by the alteration of pre-existing micas, illites, volcanic glass, hydrothermal action, and diagenetic alteration of smectite. Moreover, these are also formed by leaching of potassium (K) from micas and illites during intense continental weathering. Mixed-layered illite-smectite clay minerals also typically form by illitization of smectite during burial diagenesis or hydrothermal alteration at elevated temperatures. Kaolinite is also illitized and even detrital muscovite alters to sericite (illite or I-S) (McDowell and Elders, 1980). As for examples, (i) detrital muscovite → sericite (I-S or illite) → phengite→muscovite, and (ii) smectite + K-feldspar (+ mica?) → I-S + chlorite + quartz. These data suggest that I-S and/or illite have a stability field with respect to muscovite. The estimated temperatures from illite-smectites show ranging from 175° to 247°C. In this case, illitization reaction is possible and already detectable comparatively high temperature in the studied sequence (Perry and Hower, 1970). On the other hand, the occurrences of glassy materials in the studied Gondwana rocks also suggest that illite-smectite might also be formed during weathering of silicic glass at depth 560 m in GDH-40.

SEM and XRD analyses suggest that most of the chlorites are relatively iron-rich, which are mostly associated with sedimentary iron formations apparently have formed by direct precipitation. Chlorites also in these sedimentary rocks suggest their origin may be low grade metamorphic alternation from existing ferromagnesian minerals or

it may be addition of Fe, Mg or other compounds in the rocks. Some of dioctahedral chlorites have both sedimentary and hydrothermal origin. Secondary, post-depositional chlorite is a common component in marine sediments, where it commonly forms from the alteration of volcanic material or montmorillonite. Weaver (1989) noted that the Ordovician K-bentonites beds of the eastern United States, with common presence of chlorite have a dioctahedral 2:1 layer and a trioctahedral hydroxides sheets. Both layers were probably formed in place from the alteration of volcanic ash in a marine environment. It is very well-known that every Phanerozoic system has a number of K-bentonites beds, representing the episodes of Ordovician explosive volcanism. These K-bentonites gradually converted into interstratified illite–smectite clay-rich beds over time (Christidis and Huff, 2009). These types of events have also been reported from North and South America, Asia and Europe (Christidis and Huff, 2009). The volcanic events (interbedded 3~4 beds of tuffite) that yielded major smectite deposits are linked with supereruptions, which affected the global climate (Christidis and Huff, 2009). These volcanic materials might be the precursor of the studied mixed-layered illite-smectite clays (Hossain et al., 2015). The Cambrian-Ordovician orogenesis might have been actively contributed such type of materials in the Tethyan region during the assembly of Gondwana supercontinent (Myrow et al., 2006).

Presence of kaolinite is very significant to understand the nature and extent of weathering and the climatic variation prevailed during Paleozoic time. In general, kaolinite may be derived from K-feldsper, labradorite, illite and/or even from montmorillonite in an acidic environment (Kadir et al., 2011). Presence of kaolinite also indicates the prevalence of warm and humid climate in which the feldspar minerals were decomposed to clays and typical for sub-humid to humid condition in proximal fluvial sediments (Zuther et al., 2000). Kaolinites are often found in rocks that have been affected by intense hydrothermal alteration. In some cases, the formation of aggregates is related to the alteration of previously crystallized minerals/rocks (Jimenez-Millan et al., 2007). It also indicates sub-aerial weathering for the sediments in the source areas. Moreover, mixed-layered clays are also formed by leaching of K from micas and illites during intense continental weathering prevailed. Opal-CT is the most prominent non-clay minerals in the studied rocks. Absence of opal-A peak and the alternation of volcanic glass to smectite suggest a volcanogenic origin of the opal-CT in the Gondwana sequence in Barapukuria Formation. The most muscovite types suggest postmagmatic origin (Speer, 1984).

Immediately above glaciogenic tillites, dominant illite-smectite clay minerals, which are finally converted from K-bentonites or volcanic ash with some tuffaceous events, like glass shards (Fig. 4h), opal-CT, laumontite indicate volcanogenic ash deposits, which are also geographically widespread, although they generally occur sporadically in the lower Paleozoic geologic record in mostly the Deicke and Millbrig in North America, the Kinnekulle in northern Europe and Argentina (Huff et al., 1996; Huff et al., 1998). These records have been reported from Gondwana in the Argentine Precordillera, the Yangtze Platform, South China, Central Libya, Laurentia, Baltica and numerous terrains between Gondwana and Baltica (Christidis and Huff, 2009). Ordovician K-bentonite beds have a long history of investigation all around the world.

In this sequence, presence of mixed-layered illite-smectite clay minerals also typically formed by illitization of smectite during burial diagenesis or hydrothermal alteration. The overall clay mineral assemblage of the area reveals the sub-aerial weathering, chemical decomposition and mechanical fragmentation of the source rocks under humid to sub-humid climatic conditions.

On the other hand, signatures of volcanogenic materials (Fig. 1, Table 1, Fig. 3a and Fig. 4h) have enormous value as stratigraphic marker horizons in this Indian subcontinent and very important stratigraphic markers used for correlation purposes. These finding is significant not only for their value in local and regional chronostratigraphic correlation but also for global geochronology, paleogeography, paleotectonic and paleoclimatic reconstructions (Dronov et al., 2011; Hossain et al., 2015).

Acknowledgements

We are grateful to Prof. Y. Ogawa, University of Tsukuba, Japan and Prof. Sohail Kabir, University of Rajshahi, Bangladesh for their valuable suggestions. We are thankful to Director General of Geological Survey of Bangladesh (GSB), Dhaka, Bangladesh for support to XRD analysis. Special thanks are due to Dr. N. Nishida, University of Tsukuba, Japan for his assistance on microprobe analyses and Md. Aftabuzzaman for sample preparation for XRD analysis. The constructive comments of Prof. Dr. Yoji Arakawa helped to improve the manuscript.

References

Aftabuzzaman, M., Kabir, S., Islam, M.K. and Alam, M.S., 2013. Clay Mineralogy of the Pleistocene Soil Horizon in Barind Tract, Bangladesh. *Journal of Geological Society of India* **81**, 677–684.

Baker, J.C. and Golding, S.D., 1992. Occurrence and pal-

aeohydrological significance of Authigenic kaolinite in the aldebaran sandstone, Denison trough, Queensland, Australia. *Clays and Clay Minerals* **40(3)**, 273–279.

Bakr, M.A., Rahman, Q.M.A. and Islam, M.M., 1986. Barapukuria coal deposite Parbatipur Upazila, Dinajpur District. *Geological Survey Report, Bangladesh* (Unpublished).

Bakr, M.A., Rahman, Q.M.A., Islam, M.M., Islam, M.K., Uddin, M.N., Resan, S.A., Haider, M.J., Islam, M.S., Ali, M.W., Chowdhury, M.E.A., Mannan, K.H. and Anam, A.N.M.H., 1996. Geology and coal deposits of Barapukuria Basin Dinajpur district, Bangladesh. *Geological Survey Report* V. 8, part-1.

Bauer, A., Velde, B. and Berger, G., 1998. Kaolinite transformation in high molar KOH solutions. *Applied Geochemistry* **5**, 619–629.

Bentabol, M., Ruiz Cruz, M.D., Huertas, F.J. and Linares, J., 2003. Characterization of the expandable clays formed from kaolinite at 200°C. *Clay Minerals* **38**, 445–458.

Cathelineau, M., 1988. Cation site occupancy in chlorites and illites as a function of temperature. *Clay Minerals* **23**, 471–485.

Chatterjee, N.D. and Froese, E., 1975. A thermodynamic study of the pseudobinary join muscovite-paragonite in the system $KAlSi_3O_8$,-$NaAlSi_3O_8$-Al_2O_3-SiO_2-H_2O. *American Mineralogists* **60**, 985–993.

Christidis, G. E. and Huff, W. D., 2009. Geological Aspects and Genesis of Bentonites. *Elements* **5**, 93–98.

CMC (China National Machinery Import and Export Corporation), 1994. Preliminary Geology and Exploration Report of Barapukuria Coal Mine, Bangladesh (unpubl.), 174P.

Compton, S., 1991. Origin and diagenesis of clay minerals in the Monterey Formation, Santa Maria Basin Area, California. *Clays and Clay Minerals* **39(5)**, 449–466.

Dronov, A.V., Huff, W.D., Kanygin, A.V., Gonta and T.V., 2011. K-bentonites in the Upper Ordovician of the Siberian Platform. In: Gutiérrez-Marco, J.C., Rábano, I., García-Bellido, D. (eds), Ordovician of the World, pp. 135–141.

Ehrenberg, S.N. and Nadeau, P.H., 1989. Formation of Diagenetic Illite in Sandstones of the Garn Formation, Haltenbanken Area, Mid-Norwegian Continental Shelf. *Clay Minerals* **24(2)**, 233–253.

Elzea, J.M., Odom, I.E. and Miles, W.J., 1994. Distinguishing well ordered opal-CT and opal-C from high temperature cristobalite by x-ray diffraction. *Analytica Chimica Acta* **286**, 107–116.

Elzea, J.M. and Rice, S.B., 1996. TEM and X-ray diffraction evidence for Cristobalite and tridymite stacking Sequences in opal. *Clays and Clay Minerals* **44(4)**, 492–500.

Eugster, H.P., Albee, A.L., Bence, A.E., Thompson, J.B. and Waldbaum, D.R., 1972. The two-phase region and excess mixing properties of paragonite-muscovite crystalline solutions. *Journal of Petrology* **13**, 147–179.

Farhaduzzaman, M., Abdullah, W.H. and Islam, M.A., 2012. Depositional environment and hydrocarbon source potential of the Permian Gondwana Coals from the Barapukuria Basin, Northwest Bangladesh. *International Journal of Coal Geology* **90**, 162–179.

Frank-Kamenetskii, V.A., Goilo, E.A., Kotov, N.V. and Rieder, M., 1990. Structural Transformations of Kaolins into (Ni, Al) Serpentine-like Phases and Subsequently into Trioctahedral Micas under Hydrothermal Conditions (Note). *Clay Minerals* **25**, 121–125.

Frey, M., 1987. Low Temperature Metamorphism, Glasgow: Blackie, 351P.

Gibbs, R.J., 1965. Error due to segregation in quantitative clay mineral X-ray diffraction mounting techniques. *American Mineralogists* **50**, 74l–751.

Gilg, H.A., Hülmeyer, S., Miller, H. and Sheppard, S.M.F., 1999. Supergene origin of the Lastarria kaolin deposit, South-Central Chile, and paleoclimate implications. *Clays and Clay Minerals* **47**, 201–211.

Gilg, H.A., Weber, B., Kasbohm, J. and Frei, R., 2003. Isotope geochemistry and origin of illite-smectite and kaolinite from the Seilitz and Kemmlitz kaolin deposits, Saxony, Germany. *Clay Minerals* **38**, 95–112.

Gribb, A.A. and Banfield, J.F., 1997. Particle size effects on transformation kinetics and phase stability in nanocrystalline TiO_2. *American Mineralogists* **82**, 717–728.

Guthrie, G.D.,Jr, Bish, D.L. and Reynolds, R.C.,Jr, 1995. Modeling the X-ray diffraction pattern of opal-CT. *American Mineralogists* **80**, 869–872.

Hein, J.R., Scholl, D.W., Barron, J.A., Jones, M.G. and Miller, J., 1978. Diagenesis of Late Cenozoic diatomaceous deposits and formation of the bottom simulating reflector in the southern Bering Sea. *Sedimentology* **25**, 155–181.

Hossain, H.M.Z., Islam, M.S., Ahmed, S.S. and Hossain, I., 2002. Analysis of Sedimentary Facies and Depositional Environments of Permian Gondwana Sequence in Borehole GDH-45, Khalaspir Basin, Bangladesh. *Geosciences Journal* **6(3)**, 227–236.

Hossain, I., 1999. Lithofacies and petrographic study of the Gondwana Group in the Boreholes GDH-40, and GDH-43 Barapukuria Basin, Dinajpur, Bangladesh.

M.Sc. Thesis, University of Rajshahi (unpublished).

Hossain, I., Ahmed, S.S. and Islam, M.S., 2000. Provenance of Gondwana sandstones in the borehole GDH-40, Barapukuria basin, Dinajpur, Bangladesh. *Bangladesh Journal of Geology* **19**, 35–43.

Hossain, I., Tsunogae, T., Rajesh, H.M., Chen, B. and Arakawa, Y., 2007. Palaeoproterozoic U–Pb SHRIMP zircon age from basement rocks in Bangladesh: a possible remnant of Columbia supercontinent. *Comptes Rendus Geoscience* **339**, 979–986.

Hossain, I., Tsunogae, T., Islam, M.S., Roy, R.R. and Talukder, S., 2015. Glacio- and Volcanogenic Events with Palaeogeography of Gondwana Sequence in Bangladesh: Evaluation from Mineralization and Lithofacies study. *International Association for Gondwana Research Conference Series* No. 21, pp. 38–40.

Hower, J., Eslinger, E., Hower, M.E. and Perry, E.A., 1976. Mechanism of burial metamorphism of argillaceous sediment: 1. Mineralogical and chemical evidence. *Geological Society of American Bulletin* **87**, 725–737.

Huang, W-.L., 1993. The formation of illitic clays from kaolinite in KOH solution from 225°C to 350°C. *Clays and Clay Minerals* **41**, 645–654.

Huff, W.D., Bergström, S.M., Kolata, D.R., Cingolani, C.A. and Astini, R.A., 1998. Ordovician K-bentonites in the Argentine Precordillera: relations to Gondwana margin evolution. *Geological Society of London, Special Publication* **142**, 107–126.

Huff, W.D., Kolata, D.R., Bergström, S.M. and Zhang, Y-.S., 1996. Large-magnitude Middle Ordovician volcanic ash falls in North America and Europe: dimensions, emplacement and post-emplacement characteristics. *Journal of Volcanology and Geothermal Research* **73**, 285–301.

Islam, M.S., 1992. Facies analysis of the Permian Gondwana Group in the Barapukuria basin, Dinajpur, Bangladesh. *9th International Gondwana Symposium, India*, Abstract volume, p. 86.

Islam, M.S., 1996. Gondwana coal resources of Bangladesh and their characteristics. In: Khan, A.A., Huda, Q., Hossain, V. (eds), Proceedings of 2nd SEGMITE International Conference, Pakistan, 1994, pp. 85–90. (2nd SEGMITE International Conference held in 1994 but published in 1996)

Islam, M.M., Resan, S.A., Haider, M.J., Islam, M.S., Ali, M.W. and Chowdhury, M.E.A., 1987. Subsurface geology and coal deposits of Barapukuria area. Parabatipur upazila Dinajpur district, Bangladesh. *Geological Survey Report, Bangladesh* (Unpublished).

Islam, M.N., Uddin, M.N., Resan, S.A., Islam, M.S. and Ali, M.W., 1992. Geology of the Khalaspir Coal Basin, Pirganj, Rangpur, Bangladesh. *Geological Survey Report, Bangladesh* v. 6 (part-5)

Islam, M.S., 1993. Anatomy and Environment of deposition of the abnormally thick coal seam VI in the Barapukuria Basin, Dinajpur, Bangladesh. *Bangladesh Journal of Geology* **12**, 27–38.

Islam, M.S., 1994. Facies analysis of the Permian Gondwana Group in the Barapukuria Basin, Dinajpur, Bangladesh. *9th International Gondwana Symposium, Geological Survey of India*, Abstract volume, p. 86

Islam, M.S., 2001. Stratigraphy and Sedimentology of Gondwana Rocks in the Barapukuria Basin, Dinajpur District, Bangladesh. *Unpublished PhD Thesis, Jahangirnagar University, Dhaka, Bangladesh*.

Islam, M.S. and Hossain, I., 2006. Lithofacies and Embedded Markov chain Analyses of Gondwana sequence in Boreholes GDH-40, and GDH-43, Barapukuria coal field, Bangladesh. *Bangladesh Journal of Geology* **25**, 64–84.

Jimenez-Millan, J., Velilla, N. and Vazquez, M., 2007. Two-stage formation of kaolinite in shear-zone states, southern Iberian Massif, SE Spain. *Clay Minerals* **42**, 273–286.

Kadir, S., Erman, H. and Erkoyun, H., 2011. Mineralogical and Geochemical Characteristics and Genesis of Hydrothermal Kaolinite Deposits within Neogene Volcanites, Kütahya (Western Anatolia), Turkey. *Clays and Clay Minerals* **59(3)**, 250–276.

Keller, W.D., Reynolds, R.C.,Jr and Inoue, A., 1986. Morphology of clay minerals in the smectite-to-illite conversion series by scanning electron microscopy. *Clays and Clay Minerals* **34**, 187–197.

Khan, A.A. and Chouhan, R.K.S., 1996. The crustal dynamics and the tectonic trends in the Bengal Basin. *Journal of Geodynamics* **22**, 267–286.

Koporulin, V.I., 2013. Formation of Laumontite in Sedimentary Rocks: A Case Study of Sedimentary Sequences in Russia. *Lithology and Mineral Resources* **48(2)**, 122–137.

McDowell, D.S. and Elders, W.A., 1980. Authigenic layer silicate minerals in borehole Elmore 1, Salton Sea Geothermal Field, California, USA. *Contributions to Mineralogy and Petrology* **74**, 293–310.

Millot, G., 1970. Geology of clays (trans. Farrand W.R. and Paquet, H.), New York: Springer-Verlag.

Moore, D.M. and Raynold, R.C., 1989. X-ray diffraction and the identification and analysis of clay minerals, Oxford University Press, Oxford, pp. 332

Murata, K.J. and Larson, R.R., 1975. Diagenesis of Miocene siliceous Shale, Temblor Range, California. *Journal of Research of the U. S. Geological Survey* **3**, 553–566.

Myrow, P.M., Snell, K.E., Hughes, N.C., Paulsen, T.S., Heim, N.A., Parcha, S.K., 2006. Cambrian Depositional History of the Zanskar Valley Region of the Indian Himalaya: Tectonic Implications. *Journal of Sedimentary Research* **76**, 364–381.

Perry, E. and Hower, J., 1970. Burial diagenesis in Gulf Coast pelitic sediments. *Clays and Clay Minerals* **18**, 165–177.

Powell, B.N., Snyder, W.S. and Churchill, R.K., 1983. Petrogenesis and Structural and Thermal History of Core from Traenabanken 6609/7-1 Well: Final Report, 44P.

Reynolds, W.R., 1970. Mineralogy and stratigraphy of Lower Tertiary clays and claystones of Alabama. *Journal of Sedimentary Petrology* **40**, 829–838.

Senkayi, A.L., Ming, D.W., Dixon, J.B. and ye Hossner, L.R., 1987. Kaolinite, opal-CT and clinoptilolite in altered tuffs interbedded with lignite in the Jackson Group, Texas. *Clays and Clay Minerals* **35**, 281–290.

Speer, R., 1984. Micas in igneous rocks. Reviews in Mineralogy: Micas (ed. Bailey SW) *Mineralogical Society of America* **13**, 299–349.

Środoń, J., 1979. Correlation between coal and clay diagenesis in the Carboniferous of the Upper Silesion Coal Basin. *Proceeding of International Clay Conference*, Oxford, 251–260.

Środoń, J., 1999. Use of clay minerals in reconstructing geological processes; recent advances and some perspectives. *Clay Minerals* **34(1)**, 27–37.

Środoń, J. and Eberl, D.D., 1984. Illite, In: Micas (ed. Bailey SW). Reviews in Mineralogy, *Mineralogical Society of America* **13**, 495–544.

Uddin, M.N. and Islam, M.S., 1992. Gondwana basins and their coal resources in Bangladesh (Abstract). Issue of the GEOSAS-1, Pakistan, p. 30.

Velde, B. (ed), 1995. Origin and Mineralogy of Clays. Clays and the Environment. Springer, Berlin, 334P.

Wardell Armstrong Ltd., 1991. Techno-feasibility study of the Barapukuria coal project, Dinajpur, Bangladesh. Report submitted to Ministry of Energy and Mineral Resources, Government of People's Republic of Bangladesh (Unpubl.).

Weaver, C.E., 1958. The effect and geologic significance of potassium "fixation" by expandable clay minerals derived from muscovite, biotite, chlorite, and volcanic material. *American Mineralogists* **43**, 839–861.

Weaver, C.E. and Pollard, L.D., 1975. The chemistry of clay minerals. Developments in Sedimentology 15. Elsevier Scientific Publishing Company, 212P.

Weaver, C.K., 1989. Clay, muds and shales, Amsterdam: Elsevier, 819P.

Zuther, M., Brockamp, O. and Clauer, N., 2000. Composition and origin of clay minerals in Holocene sediments from the south- eastern North Sea. *Sedimentology* **47**, 119–134.